npj Computational Materials

www.nature.com/npjcompumats

REVIEW ARTICLE OPEN

Check for updates

From basic properties to the Mott design of correlated delafossites

Frank Lechermann [1,2]✉

The natural-heterostructure concept realized in delafossites highlights these layered oxides. While metallic, band- or Mott-insulating character may be associated with individual layers, inter-layer coupling still plays a decisive role. We review the correlated electronic structure of $PdCoO_2$, $PdCrO_2$, and $AgCrO_2$, showing that layer-entangled electronic states can deviate from standard classifications of interacting systems. This finding opens up possibilities for materials design in a subtle Mott-critical regime. Manipulated Hidden-Mott physics, correlation-induced semimetallicity, or Dirac/flat-band dispersions in a Mott background are emerging features. Together with achievements in the experimental preparation, this inaugurates an exciting research field in the arena of correlated materials.

npj Computational Materials (2021)7:120 ; https://doi.org/10.1038/s41524-021-00586-6

INTRODUCTION

A common statement on the research on strongly correlated materials, especially from a theory perspective, refers to the fact that the body of compounds that fall into this category is rather small, and hence the relevance and impact in general materials science scales accordingly. While there has been some truth in this view, there are also obvious facts that argue against. First undoubtedly, the properties of various correlated systems are singular. High-temperature superconductivity in cuprates or colossal magnetoresistance in manganites are only two extraordinary features that stand out in condensed matter physics. Moreover, even 'straightforward' materials properties, such as e.g., magnetism in the solid state, are often relying on some effect of electronic correlation. Second, times are changing and from an applicative viewpoint, understanding and engineering electron correlation may be indispensable to make progress in battery materials, thermoelectric devices, photovoltaic systems, data-storage media and other sorts of 'smart' materials. Against this background, we want to discuss in this overview the fascinating physics of a certain class of transition-metal (TM) oxides prone to correlation effects, namely the delafossites[1–5]. Importantly, this materials class is not only of interest due to its intrinsic basic properties, but also because of the potential for even more intriguing characteristics upon further design.

In order to theoretically investigate challenging systems with subtle electronic characteristics, an advanced framework is needed, capable of addressing electron states from weak to strong correlation on an equal footing. Model-Hamiltonian approaches may only be used at a later stage, when focussing on certain details of the complex quantum problem. Density functional theory (DFT) in Kohn-Sham representation is proper to describe the band formation from first principles, but will not be sufficient to account for relevant correlation effects. The combination of DFT with dynamical mean-field theory (DMFT), the so-called DFT+DMFT method[6–8], is well suited for the problem, as it can account for site- and orbital-resolved Mott criticality at strong coupling as well as for mildly renormalized dispersions at weak coupling in a realistic setting.

Delafossites, named after the french crystallographer Gabriel Delafosse (1796–1878), are in fact known for quite some time. The first delafossite, the $CuFeO_2$ mineral, has been discovered[1] near Yekaterinburg, Russia, in 1873 and then re-discovered[2] near Bisbee(Arizona), USA, in 1913. Since then, numerous compounds of the delafossite-oxide type $\mathcal{A}\mathcal{B}O_2$, where $\mathcal{A}$ and $\mathcal{B}$ denote different metallic elements, have been crystallized. The unique crystal structure (see Fig. 1) consists of an alternate stacking of triangular $\mathcal{A}$ lattices and planes of edge-sharing $\mathcal{B}O_6$ octahedra along the *c*-axis, whereby these two different layer types are connected via oxygen in a so-called dumbbell position. There are two possible stacking scenarios, namely the more common rhombohedral one with $R\bar{3}m$ space-group symmetry and the hexagonal one giving rise to $P6_3/mmc$ symmetry. The metallic ions are in the formal oxidation state $\mathcal{A}^+$ and $\mathcal{B}^{3+}$, respectively.

Delafossites are divided into a larger insulating and a smaller metallic class of compounds. In modern times, the *p*-type electrical conduction in the transparent $CuAlO_2$ insulator[9] gained strongest interest. In a series of papers[3–5], Shannon et al. in 1971 described the novel synthesis and single-crystal growth of several delafossites with $\mathcal{A}$=Pd, Pt and Ag. Among those, there are oxides with exceptionally high electrical conductivity at room temperature, e.g., $PdCoO_2$ and $PtCoO_2$, in combination with an outstanding single-crystal purity. This combined feature found in a selected subgroup of delafossites has started to become an intense field of research (see e.g., Refs. [10,11] for reviews). This elitist group of delafossites in terms of metallic properties, includes the $PdCrO_2$ compound, which, among further challenging physics, hosts Mott-insulating CrO_2 layers[12–14].

This brings us to a very relevant aspect. The special delafossite architecture gives rise to a natural heterostructure, in which individual layers may attain a distinct character of their own. In most layered materials, e.g., cuprates, cobaltates, etc., there is usually one 'active' layer type and the remaining part mainly provides the glue. However in delafossites, e.g., the $\mathcal{A}$ layer can manage the metallic transport, while the $\mathcal{B}O_2$ layers account for the magnetic ordering. This not only entails exciting physical processes in the pure compound, but furthermore allows for a

[1]European XFEL, Schenefeld, Germany. [2]Center for Computational Quantum Physics, Flatiron Institute, New York, NY, USA. ✉email: frank.lechermann@xfel.eu

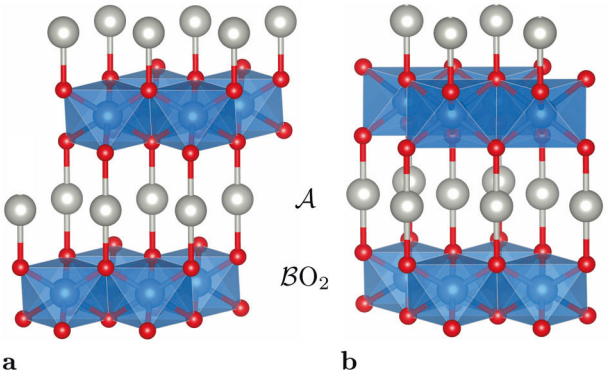

Fig. 1 Delafossite $\mathcal{AB}O_2$ crystal structure. (**a**) $R\bar{3}m$ and (**b**) $P6_3/mmc$ symmetry. $\mathcal{A}$ (grey), $\mathcal{B}$ (blue) and O (red).

kind of 'meta oxide-heterostructure' physics upon additional (nano-)engineering.

Since the family of delafossites encircles a vast number of compounds with many different physical aspects, we cannot reasonably-well cover all those in this comparatively brief treatise. Instead, the goal is to focus on the specific role of electron correlations in selected compounds with $\mathcal{A}$=Pd, Ag and $\mathcal{B}$=Co, Cr as well as an assessment of possible designing routes. For further discussion of delafossites we refer the reader to the exisiting body of literature, e.g., Refs. [10,11,15–17] and references therein.

One usually refers to the term "Mottness" in order to mark the phenomenology of an electronic system either close to a Coulomb-interaction driven metal-to-insulator transition or already in a Mott-insulating state. It most often includes e.g., abrupt changes in transport behavior, unique temperature dependencies and/or strong magnetic response due to the formation/existence of local moments. As a rule of thumb, the poorly screened Coulomb interaction exceeds (or is comparabale to) the relevant bandwidth in corresponding materials. In TM oxides, there are various cases that give rise to Mottness, which depend on certain properties of the TM ion and the actual crystal structure (see e.g., Ref. [18] and references therein for a detailed review).

When starting from a non-interacting metallic band structure, in conventional cases a given band manifold crossing the Fermi level is subject to Coulomb interactions that arise locally from the TM site, i.e., associated with a Hubbard U. The size of the orbital space that defines this specific band manifold as well as its filling are crucial properties. The one-band/one-orbital limit, though most appreciated from a model perspective, is however very rarely realized in concrete materials. Further key property is the placement of the TM element in the periodic table, which regulates the TM(d) vs. O($2p$) level position[19]: strongly correlated early TM oxides are mostly of Mott-Hubbard type, whereas such late TM oxides are mostly of charge-transfer type. Moreover, the correlation signatures depend on the TM-element row. For instance, spin-orbit effect are often non-negligible in 4d and especially 5d oxides, whereby the corresponding U values are usually smaller than in 3d oxides.

Then there are more detailed differentiations that arise from specific compound characteristics. For instance, in orbital-selective Mott systems[20] only a subclass of the relevant orbitals become Mott critical. Explicit non-local correlation effects, e.g., on selected short-range bonds, play a key role in a few materials[21]. Doping with impurities can lead to novel behavior, e.g., the appearance of site-selective Mott behavior where interaction-driven localization tendencies occurs only on selected lattice sites[22]. Last but not least, so-called Hund metals (see[23] for a review) are in principle distant from a Mott-critical regime, but enable features of strong correlation based on an interplay of U and the Hund's exchange J_H. While Mottness is usually strongest for half-filled orbital manifolds, the latter "Hundness" is usually strongest for orbital manifolds with one electron(hole) added to half filling.

Notably, electronic correlation in selected delafossites adds a further scenario to the list. Their specific layered structure can account for layer-selective Mott criticality that may furthermore be connected to singular layer-to-layer coupling. This means that only certain layers within the delafossite structure are in or close to a Mott state, whereas remaining layers are well conducting. This kind of selectivity can on the other hand give rise to non-conventional quantum states for electrons that want to move coherently throughout the complete system.

Before delving into the details of the correlated electronic structure of delafossites, a reminder of the state-of-the-art DFT+DMFT approach is given in the following section. Since this review is intended to focus on the materials and the correlation-design aspect, that theory part will be rather brief. There are already various more extensive descriptions of DFT+DMFT,[8,24,25].

DENSITY FUNCTIONAL THEORY PLUS DYNAMICAL MEAN-FIELD THEORY

General formalism

Describing the general many-body problem from weak to strong coupling in a condensed matter system within a first-principles (-like) manner is tough. A unique and well-defined solution has not been given yet. Especially when one also wants to address materials science questions with larger unit cells and larger orbital manifolds, a solution presumably has to wait for much longer times. Approximate hybrid methods that divide the complex problem into (coupled) subproblems of different significance have proven adequate to obtain good results beyond effective single-particle schemes. The DFT+DMFT technique is such a hybrid method. We assume that the reader is familiar with DFT and we note that the term 'DFT' is understood throughtout the text as 'effective single-particle Kohn-Sham DFT'. While this discrimination is important, we here focus on practical calculations and shorten the abbrevation for readability matters.

The dynamical mean-field theory[26,27] was invented for model Hamiltonians and is appreciated as the many-body scheme with the best compromise between generality, accuracy and performance. Just as Kohn-Sham DFT, also DMFT describes a mapping: from the problem of interacting lattice electrons onto the problem of a quantum impurity within a self-consistent energy-dependent bath, sketched in Fig. 2a. Key focus is on the one-particle Green's function, which for chemical potential μ and Hamiltonian $H(\mathbf{k})$ at wave vector $\mathbf{k}$ reads

$$G(\mathbf{k}, i\omega_n) = [i\omega_n + \mu - H(\mathbf{k}) - \Sigma(\mathbf{k}, i\omega_n)]^{-1} \quad . \tag{1}$$

Note that here, fermionic Matsubara frequencies $\omega_n := (2n+1)\pi T$ are employed to emphasize the treatment at finite temperature. The analytical continuation to real frequencies ω in actual calculations may e.g., be performed via the maximum entropy method (see[18,28,29] for more details). The self-energy Σ describes the many-body part of the problem, and hence, finding a good approximation is key to a physically sound picture. In DFT, the self-energy is approximated, in essence, by the energy-independent sum of Hartree potential v_H and exchange-correlation potential v_{xc} in the form of a simple forward-scattering term. In DMFT, the local Green's function is approximated with the help of a $\mathbf{k}$-independent but energy-dependent impurity self-energy $\Sigma_{imp}(i\omega_n)$, i.e.,

$$G_{loc}^{DMFT}(i\omega_n) = \sum_{\mathbf{k}} [i\omega_n + \mu - H(\mathbf{k}) - \Sigma_{imp}(i\omega_n)]^{-1} \quad , \tag{2}$$

whereby the corresponding impurity problem is defined via

$$\Sigma_{imp}(i\omega_n) = \mathcal{G}_0(i\omega_n)^{-1} - G_{imp}(i\omega_n)^{-1} \quad . \tag{3}$$

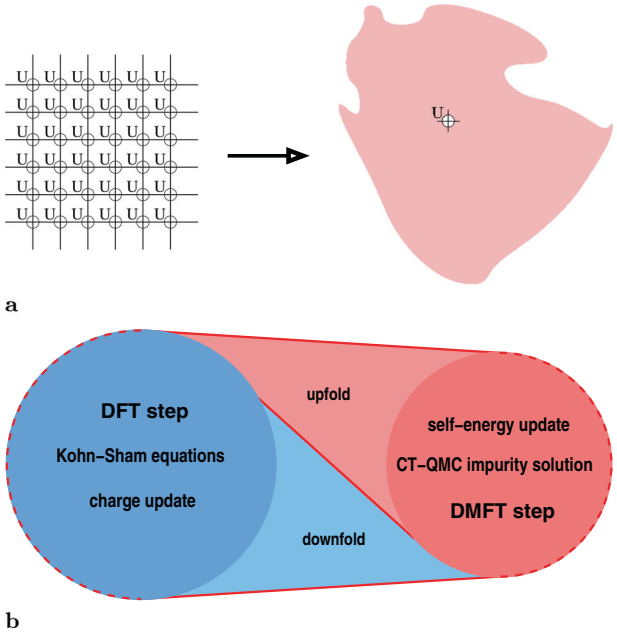

Fig. 2 Basics of the realistic-DMFT framework. a Sketch of the DMFT mapping. An interacting electron system on a lattice with a Coulomb repulsion U on each site is mapped onto a single interacting site in an energy-dependent bath. The latter is determined self-consistently in an iterative cycle. **b** State-of-the-art charge self-consistent DFT+DMFT loop (after[38]). The calculation usually starts from a self-consistent Kohn-Sham solution. The correlated subspace is defined and the initial Weiss field $\mathcal{G}_0$ constructed. Afterwards, a single DMFT step is performed. The obtained self-energies are upfolded and an updated charge density $n(\mathbf{r})$ is computed. A new charge density implies a new Kohn-Sham potential, and a single new Kohn-Sham step is performed, therefrom a new Weiss field is generated, etc.

The Weiss field $\mathcal{G}_0(i\omega_n)$ is a function of the local Hamiltonian (expressed within a localized basis). The important DMFT self-consistency condition implies $G_{\rm imp} = G_{\rm loc}^{\rm DMFT}$ and is usually achieved within a loop, just as the Kohn-Sham cycle. From an initial version of $\mathcal{G}_0$, the self-energy $\Sigma_{\rm imp}$ is determined and with the use of (2),(3) a new $\mathcal{G}_0$ extracted, and so on. The hard part consists in solving the quantum-impurity problem to obtain $G_{\rm imp}$ for a given Weiss field. So-called 'solvers' based e.g., on quantum Monte Carlo, Exact Diagonalization, etc. are employed for that task. Note that local-interaction diagrams are included to all orders in this non-perturbative theory. The vital energy dependence of the Weiss field ensures the qualitatively correct description of low-energy quasiparticle (QP) features as well as high-energy incoherent (Hubbard) excitations. Extensions to overcome the restriction to a local self-energy, e.g., via cluster schemes, are available, but will not be pursued here.

We now come back to the portioning into subspaces within DFT+DMFT. Concerning DFT for a few hundred sites, there is no issue for conventional exchange-correlation functionals and one may apply that approach to the complete electronic Hilbert space. This ensures a reliable description of the bonding, band formation and screening properties in a given material. On the other hand, DMFT as a manifest many-body scheme is not applicable to hundreds of sites. Furthermore and very importantly, there are further issues to the use of pure DMFT in a concrete materials context. First, DMFT builds up on the physics of interactions in orbitals with reasonably local character, i.e., a Hubbard-model-like scenario. However, such a scenario is not straightforwardly suitable for e.g., dominant s and p electron states. Second, DMFT is designed to provide proper access to the self-energy Σ, but not to derive general hoppings t. In other words, a full-monty DMFT starting from atomic Coulomb potentials on a given lattice is just not the conventional modus operandi. Note that there are ideas to use DMFT for quantum chemistry problems in a direct manner[30,31], but it is still a long way to condensed matter materials science. Therefore, putting materials-oriented DMFT into practise is currently best done by allocating a restricted Hilbert subspace, i.e., the so-called correlated subspace.

The correlated subspace is understood as a quantum-numbered real-space region where correlated electrons reside. Note that this subspace is not uniquely defined, but is a matter of choice in a concrete materials problem. For instance, in the case of an early transition-metal oxide, like e.g., $SrVO_3$ or V_2O_3, it may consist of the low-energy t_{2g} orbitals of the TM site(s). Within the correlated subspace, a multi-orbital interacting Hamiltonian is applied. More concretely, the corresponding Hamiltonian terms are explicitly exploited in the impurity solver. The Hamiltonian is usually of generalized Hubbard type, with local interaction parameters based on the Coulumb integral U and the Hund exchange $J_{\rm H}$. Those are either chosen by hand or computed ab-initio, e.g via the constrained random-phase approximation[32].

Key interfaces of the complete DFT+DMFT self-consistency cycle[33–36] (cf. Fig. 2b) are marked by the downfolding of the full-problem Bloch (bl) space to the correlated subspace, and the upfolding of the DMFT self-energy back to the full space. In terms of the Green's function G and the self-energy Σ, for sites $\mathbf{R}$, local orbitals mm' and band indices $\nu\nu'$ this reads formula-wise

$$G^{\mathbf{R},\rm imp}_{mm'}(i\omega_n) = \sum_{\mathbf{k},(\nu\nu')\in\mathcal{W}} \overline{P}^{\mathbf{R}}_{m\nu}(\mathbf{k})\; G^{\rm bl}_{\nu\nu'}(\mathbf{k}, i\omega_n)\; \overline{P}^{\mathbf{R}*}_{\nu'm'}(\mathbf{k})\;, \tag{4}$$

$$\Delta\Sigma^{\rm bl}_{\nu\nu'}(\mathbf{k}, i\omega_n) = \sum_{\mathbf{R},mm'} \overline{P}^{\mathbf{R}*}_{\nu m}(\mathbf{k})\; \Delta\Sigma^{\mathbf{R},\rm imp}_{mm'}(i\omega_n)\; \overline{P}^{\mathbf{R}}_{m'\nu'}(\mathbf{k})\;, \tag{5}$$

with $\overline{P}$ denoting the normalized projection between Bloch space and correlated subspace[37]. Note that Eq. (4) is necessary to define the notion of a local Green's function (eq. (2)) for the DMFT problem. As for the correlated subspace, there is a choice for the range $\mathcal{W}$ of included Kohn-Sham bands in the downfolding. The object $\Delta\Sigma^{\rm bloch}_{\nu\nu'}$ describes the $\mathbf{k}$-dependent self-energy in Bloch space after a double-counting correction. The latter takes care of the fact that some correlations are already handled on the DFT level. In the upfolding operation, the charge density $n(\mathbf{r})$ is then decorated with DMFT correlations, i.e.,

$$n(\mathbf{r}) = \sum_{\mathbf{k},\nu\nu'} \langle\mathbf{r}|\Psi_{\mathbf{k}\nu}\rangle \big(f(\tilde{\epsilon}_{\mathbf{k}\nu})\delta_{\nu\nu'} + \Delta N_{\nu\nu'}(\mathbf{k})\big)\langle\Psi_{\mathbf{k}\nu'}|\mathbf{r}\rangle \quad , \tag{6}$$

where Ψ denotes Kohn-Sham states, f marks the associated Fermi function and ΔN refers to the DMFT Bloch-density term[37,38]. A pure band picture is not adequate for a many-body system and real-space excitations also matter. Therefore, additional off-diagonal terms in the band index contribute in the correlated regime. This extended charge-density formulation accordingly then defines a new Kohn-Sham potential. Let us finally iterate on the fact that this realistic many-body scheme works, at heart, at finite temperature T. Electron states are subject to the full thermal impact, beyond sole occupational Fermi-function modification. For more formal accounts on the DFT+DMFT scheme, we refer to[8,24].

In various problems of multi-atom unit cells, the correlated subspace encircles not only a single lattice site. For symmetry-equivalent sites, the self-energy is determined for a representative site and transferred to the remaining sites via proper symmetry relations. An impurity problem is defined for each symmetry-inequivalent site j through[39]

$$\mathcal{G}^{(j)}_0(i\omega_n)^{-1} = G^{(j)}(i\omega_n)^{-1} + \Sigma^{(j)}_{\rm imp}(i\omega_n) \quad , \tag{7}$$

and the coupling is realized via the DFT+DMFT self-consistency

condition invoking the computation of the complete lattice Green's function.

This concludes the brief sketch of the charge self-consistent DFT+DMFT methodology[33,35,36]. In the next subsection, we turn to the actually chosen representation to tackle delafossites.

Concrete setting for delafossites

Charge self-consistent DFT+DMFT is employed for all electronic structure problems discussed and addressed in this overview for $\mathcal{A}\mathcal{B}O_2$-based delafossite. A mixed-basis pseudopotential method[40–42], based on norm-conserving pseudopotentials and a combined basis of localized functions and plane waves is used for the DFT part. The generalized-gradient approximation in form of the PBE functional[43] is utilized for the exchange-correlation functional. Within the mixed basis, localized functions for the transition-metal 3*d* and 4*d* shells, as well as for O(2*s*,2*p*) are used to reduce the plane-wave energy cutoff. The latter is set to 20 Ry for the bulk systems, and to 16 Ry for the heterostructures. The *k*-point mesh amounts to $13\times13\times13$ for the bulk and $11\times11\times3$ ($9\times9\times5$) for out-of-plane(in-plane) heterostructures, respectively. For all systems, the experimental lattice parameters are adopted and the internal degree of freedom *z*, governing the oxygen distance to the $\mathcal{A}$ plane, is obtained from DFT structural optimization (see Table 1).

We choose the correlated subspace to be build up from the five effective $\mathcal{B}$-site Wannier-like 3*d* functions as obtained from the projected-local-orbital formalism[37,44], using as projection functions the linear combinations of atomic 3*d* orbitals which diagonalize the $\mathcal{B}$-site 3*d* orbital-density matrix. As it will be seen later, the most-relevant correlated states in delafossites are of threefold t_{2g} kind. However, due to the subtle hybridization between two different TM sites and our further designing perspective, we stick to the more general full $3d=\{t_{2g},e_g\}$ fivefold throughout the presented results. For selected aspects, a reduction of the correlated subspace to the t_{2g} sector might still be an acceptable approximation.

A five-orbital Slater-Kanamori Hubbard Hamiltonian, i.e., including density–density, spin-flip and pair-hopping terms, is utilized in the correlated subspace, parametrized by a Hubbard *U* and a Hund exchange J_H. It reads for orbitals m,m'

$$\begin{aligned} H_\mathrm{int} = {} & U\sum_m n_{m\uparrow}n_{m\downarrow} + \tfrac{1}{2}\sum_{m\neq m',\sigma}\Big\{(U-2J_\mathrm{H})\; n_{m\sigma}n_{m'\bar{\sigma}} \\ & +(U-3J_\mathrm{H})\; n_{m\sigma}n_{m'\sigma} \\ & +J_\mathrm{H}\left(c^\dagger_{m\sigma}c^\dagger_{m'\bar{\sigma}}c_{m\bar{\sigma}}c_{m'\sigma}+c^\dagger_{m\sigma}c^\dagger_{m\bar{\sigma}}c_{m'\bar{\sigma}}c_{m'\sigma}\right)\Big\}\;, \end{aligned} \tag{8}$$

with $c^{(\dagger)}_{m\sigma}$ as the annihilation(creation) operator for spin flavor $\sigma=\uparrow,\downarrow$, and $n=c^\dagger c$. Our $\mathcal{B}$ site will here be either of Co or Cr type and a value of $J_\mathrm{H}=0.7$ eV is proper for TM oxides of that kind. Hubbard *U* values between 3−4 eV will be chosen according to adequate onsite Coulomb integrals for similiar types of oxides[45,46]. Note that no further Hubbard interactions are assigned to the $\mathcal{A}$ site. The *d* orbitals on those sites will be here of 4*d* kind, of formal d^9 filling and only weakly hybridizing with oxygen. Thus by any means, Coulomb interactions are expected much smaller than on the $\mathcal{B}$ site. Spin-orbit coupling is neglected in the crystal calculations.

Table 1. Experimental lattice parameters[3–5,59] of the studied bulk delafossites, as well as the DFT optimized internal *z* degree of freedom.

compound	*a* in Å	*c* in Å	*z*
$PdCoO_2$	2.830	17.743	0.1132
$PdCrO_2$	2.930	18.087	0.1101
$AgCrO_2$	2.985	18.510	0.1095

The encountered DMFT impurity problems in the examined delafossite materials are solved by the continuous-time quantum Monte Carlo scheme of hybridization-expansion form[47,48] as implemented in the TRIQS package[49,50]. A double-counting correction of fully-localized-limit type[51], utilizing iterated TM(3*d*) occupations, is applied in all calculations. To obtain the spectral information, analytical continuation from Matsubara space via the maximum-entropy method[29] as well as the Padé method[52] is performed. Though the $\mathcal{A}CrO_2$ delafossites order antiferromagnetically at low temperatures within the CrO_2 layers, our investigations remain at still higher temperatures and assume paramagnetism for all studied cases. If not otherwise stated, the system temperature is set to $T=290$ K.

BASIC PROPERTIES OF COO_2-BASED AND CRO_2-BASED DELAFOSSITES

General considerations

The delafossites $PdCoO_2$, $PtCoO_2$, and $PdCrO_2$ are metals with surprisingly high conductivity (see e.g., Refs. [10,11] for recent reviews). With an in-plane resistivity of 2.6 $\mu\Omega$cm[53], the $PdCoO_2$ compound is designated as the most-conductive oxide at room temperature. It apparently shows hydrodynamic flow of electrons[54]. Although obviously also a correlation effect[55], this feature will not be directly addressed in the present text, but further information can be found in Refs. [56–58] and references therein. The $AgCrO_2$ delafossite is an insulator with a charge gap of $\Delta=1.68$ eV[59]. While no ordering transition takes place in the Co compounds down to lowest temperatures, the Cr compounds display magnetic transitions into an antiferromagnetic (AFM) 120° phase below the Néel temperatures 37.5 K ($PdCrO_2$)[60] and 21 K ($AgCrO_2$)[61,62].

From symmetry, the local electronic *d*-shell states on $\mathcal{A}$ and $\mathcal{B}$ sites show a trigonal splitting into $t_{2g}=\{a_{1g},e'_g\}$ and e_g classes (see also Ref. [63]). The e'_g and e_g states are doubly degenerate, respectively. The symmetry-adapted orbitals $|m_{\mathcal{A},\mathcal{B}}\rangle$ may be expressed as linear combinations of the atomic *d* orbitals. Note that we choose the *x*,*y*-axis parallel to and the *z*-axis perpendicular to the delafossite layers. On the $\mathcal{A}$ site, there is a one-to-one matching between crystal-field orbitals and atomic orbitals, i.e., $|a_{1g}\rangle=|d_{z^2}\rangle$, $|e'_g(1,2)\rangle=|d_{xz},d_{yz}\rangle$, $|e_g(1,2)\rangle=|d_{xy},d_{x^2-y^2}\rangle$. On the $\mathcal{B}$ site, the identification is based on the usual trigonal representation, reading

$$\begin{pmatrix}|a_{1g}\rangle\\|e'_g(1)\rangle\\|e'_g(2)\rangle\\|e_g(1)\rangle\\|e_g(2)\rangle\end{pmatrix}=\begin{pmatrix}1&0&0&0&0\\0&a&0&b&0\\0&0&-a&0&b\\0&0&b&0&a\\0&b&0&-a&0\end{pmatrix}\begin{pmatrix}|d_{z^2}\rangle\\|d_{xz}\rangle\\|d_{yz}\rangle\\|d_{xy}\rangle\\|d_{x^2-y^2}\rangle\end{pmatrix}. \tag{9}$$

The values a,b may be obtained from diagonalizing the DFT orbital density matrix for the respective 3*d* shell after convergence of the crystal calculation. The nominal $\mathcal{B}^{3+}$ ion is usually in a low-spin configuration with its e_g states higher in energy and mostly empty. The collected DFT crystal-field levels of the *d* states on the respective $\mathcal{A}$ and $\mathcal{B}$ sites, along with the a,b coeffcients, are given in Table 2.

Spin-orbit effects are assumed not to play a decisive role for the transport properties, however, they might have some influence in the magnetically ordered phases. The Co ion with configuration $Co^{3+}(3d^6)$ has a closed t_{2g} subshell in the local limit, which explains the absence of magnetic ordering in (Pd,Pt)CoO_2. On the other hand, $Cr^{3+}(3d^3)$ has a half-filled t_{2g} subshell in that limit. Therefore, correlation effects, which should predominantly originate from the TM(3*d*) ions, are naturally expected stronger for

Table 2. DFT crystal-field levels on $\mathcal{A}$ (first row) and $\mathcal{B}$ (second row) site in the investigated delafossites, as well as orbital coefficients a, b on the $\mathcal{B}$ site. All energies in meV.

compound	$\varepsilon^{\mathcal{A},\mathcal{B}}_{a_{1g}}$	$\varepsilon^{\mathcal{A},\mathcal{B}}_{e'_g}$	$\varepsilon^{\mathcal{A},\mathcal{B}}_{e_g}$	a	b
	−1082	−2177	−1953		
$PdCoO_2$	−1320	−1415	−465	0.621	0.784
	−969	−2057	−1847		
$PdCrO_2$	−336	−493	831	0.586	0.810
	−3195	−4139	−4080		
$AgCrO_2$	−249	−459	743	0.548	0.837

(Pd,Ag)CrO_2. On the $\mathcal{A}$ sites, formally, the Pd ions have a $4d^9$ and the Ag ions a $4d^{10}$ oxidation state. Because of the filled Ag(4*d*) shell and the insulating nature, the Cr electrons in $AgCrO_2$ are localized in a Mott fashion. Hence, $AgCrO_2$ is a combined 'band-Mott' insulator.

In view of some general Mott-relevant classifications given in the Introduction, one can state that the Co,Cr(3*d*)-derived states are of multiorbital type, at or very close to half filling and expectedly located in a Mott-Hubbard rather than charge-transfer regime. Significant orbital-selective or Hund-metal tendencies are also not expected because of weak orbital differentiation and the half-filled nature. In the following, we will first discuss the more detailed electronic structure of $PdCoO_2$, $PdCrO_2$ and $AgCrO_2$ from a nonmagnetic Kohn-Sham DFT viewpoint. Previous DFT accounts of these system may be found e.g., in Refs. [12,16,63–68].

DFT picture

For $PdCoO_2$, Fig. 3a,b display the spectral DFT properties, namely density of states (DOS) and band structure of this metallic delafossite, as well as provide plots of the Wannier-like Pd(4*d*) orbitals. As expected, the Pd(4*d*) states are largely occupied with a bandwidth (W) hierachy of $W_{a_{1g}} > W_{e'_g} > W_{e_g}$. As shown in Fig. 3b, the Co(3*d*) weight is mostly located in the bands close to and above the Fermi level ε_F, with a single band crossing ε_F. The latter dispersion, which we denote in the following 'cPd', is dominantly of mixed Pd(4*d*) and partial Co(3*d*) kind. In more detail from the Pd site, Pd-a_{1g} and Pd-e'_g have a comparable weight on the ε_F-crossing regime of that most-relevant band. Note that the e'_g orbitals are the ones with the strongest in-plane character (see Fig. 3b). As a further note, though the band-filling Co(3*d*) character resembles the original Co($3d^6$) picture, from the hybridizations at the Fermi level a completely inert Co-t_{2g} subshell is not truly justified. The DFT fermiology and dispersions at low energy are in good agreement with data from angle-resolved photoemission spectroscopy (ARPES) measurements[69] and de Haas-van Alphen studies[53]. Thus plain DFT seemingly provides already an adequate description of key $PdCoO_2$ features.

The spectral DFT properties of $PdCrO_2$ are shown in Fig. 3c,d. Contrary to $PdCoO_2$, the $\mathcal{B}$-site states of Cr(3*d*) character are much less filled, and the three t_{2g}-dominated bands are right at the Fermi level. On the other hand, the Pd(4*d*) character at ε_F is minor. This low-energy picture of the dispersions however strongly disagrees with available experimental data from ARPES[12,66] and quantum oscillations[70,71]. In experiment, there is also only a single band crossing the Fermi level, quite similarly as in $PdCoO_2$. This discrepancy is due to the neglect of strong electronic correlations in conventional DFT, which misses the Mott-localized character of the CrO_2 layers. Partial agreement with experiment concerning the dispersions can be achieved within spin-polarized DFT[12,65,66,68], accounting also for the magnetic ordering at low temperatures. But this Slater-type handling of the Cr(3*d*) states is not truly describing the underlying physics correctly. For instance, the single cPd dispersion holds for temperatures well above the magnetic-ordering temperature[66], therefore the gapping of Cr(3*d*) is not linked to ordered magnetism.

Finally, the $AgCrO_2$ compound would be insulating in DFT if the Cr-t_{2g} states were not located again at the Fermi level (see Fig. 3e, f). The Ag(4*d*) states are filled and would give rise to a band insulator. The missing correlation effects on Cr become most evident in this delafossite. Note the prominent Ag-a_{1g} dominated band just below the Cr-t_{2g} bands in energy and with a nearly flat dispersion along K-M. It bears striking resemblance to the former low-energy cPd band in $PdCoO_2$. In fact as we will see in the following, this present band will just form the highest valence band in true $AgCrO_2$ once correlations are properly included. Furthermore for the same reason, the akin band in $PdCrO_2$ (yet there with stronger Pd-e'_g character) will be shifted to ε_F, giving rise to the experimentally revealed single-sheet fermiology.

DFT+DMFT picture

Let us now turn to an improved description of the given delafossites, arising from the inclusion of correlation effects within DFT+DMFT. Concerning the Hubbard interaction, the value $U = 3$ eV is assigned to the 3*d* states of Co and Cr in $PdCoO_2$ and $PdCrO_2$, respectively. For Cr(3*d*) in $AgCrO_2$, the somewhat larger value of $U = 4$ eV is used in order to comply with the weaker screening because of the (nearly) filled Ag(4*d*) shell. A larger part of this subsection builds up on results and discussions provided in Refs. [13,72].

Figure 4 exhibits the spectral summary for the three compounds. In the case of the Co compound, the changes compared to DFT appear minor, as already expected from the simplest picture of a closed Co-t_{2g} subshell. The dispersions, which now describe true quasiparticle features, are hardly modified at lower energy. Quite on the contrary, the QP dispersion for $PdCrO_2$ has changed dramatically (see Fig. 4b); the DFT-original Cr bands at ε_F have disappeared and instead, a single cPd dispersion as in $PdCoO_2$ crosses the Fermi level. This result brings theory eventually in line with experimental findings[12,66,70,71]. Also for $AgCrO_2$, the DFT+DMFT approach settles the comparison with experiment, namely by identifying the insulating nature with a compatible gap of ~1.8 eV. While the latter delafossite shows of course no Fermi surface, the fermiology of $PdCoO_2$ and $PdCrO_2$ in Fig. 4d, e becomes rather similar with interactions. A single-sheet interacting Fermi surface, comprising a single electron, is centered around Γ and has a hexagonal shape with some warping. Note that this warping is somewhat stronger in the case of the Co compound.

Two functions are provided to discuss the **k**-integrated spectra (see Fig. 4h–j). First, the site- and orbital projected spectral function $A_{\mathrm{proj}}(\omega)$, defined by projecting the Bloch-resolved spectral function $A_\nu(\mathbf{k}, \omega)$ with Bloch index ν onto a chosen site-orbital and summing over $\nu, \mathbf{k}$. Note that this function is comparable but strictly not identical to the local spectral function A_{loc}, which is obtained from analytical continuation of the local Green's function. Second, it proves instructive to also plot directly $A_\nu(\omega)$, i.e., the **k**-integrated Bloch-resolved spectrum. This allows us to trace the behavior of the former DFT bands upon interaction and displays the QP formation originating in Bloch space.

The projected spectrum of $PdCoO_2$ exhibits the near subshell filling of Co(3*d*) and the Pd dominance of the low-energy QP peak at the Fermi level. While on a first glance, A_{proj} for the Cr(3*d*) spectrum in $PdCrO_2$ looks similar to the previous Co(3*d*) one, the physics is completely different; the Cr-t_{2g} states are in a Mott state and therefore their spectral weight is shifted to deeper energies up and below the Fermi level, i.e., to upper and lower Hubbard bands. The Cr-e_g states are mostly empty, but show also strong incoherence effects in Fig. 4b. Mott criticality in the CrO_2 layers has been originally suggested by several experiments from strong

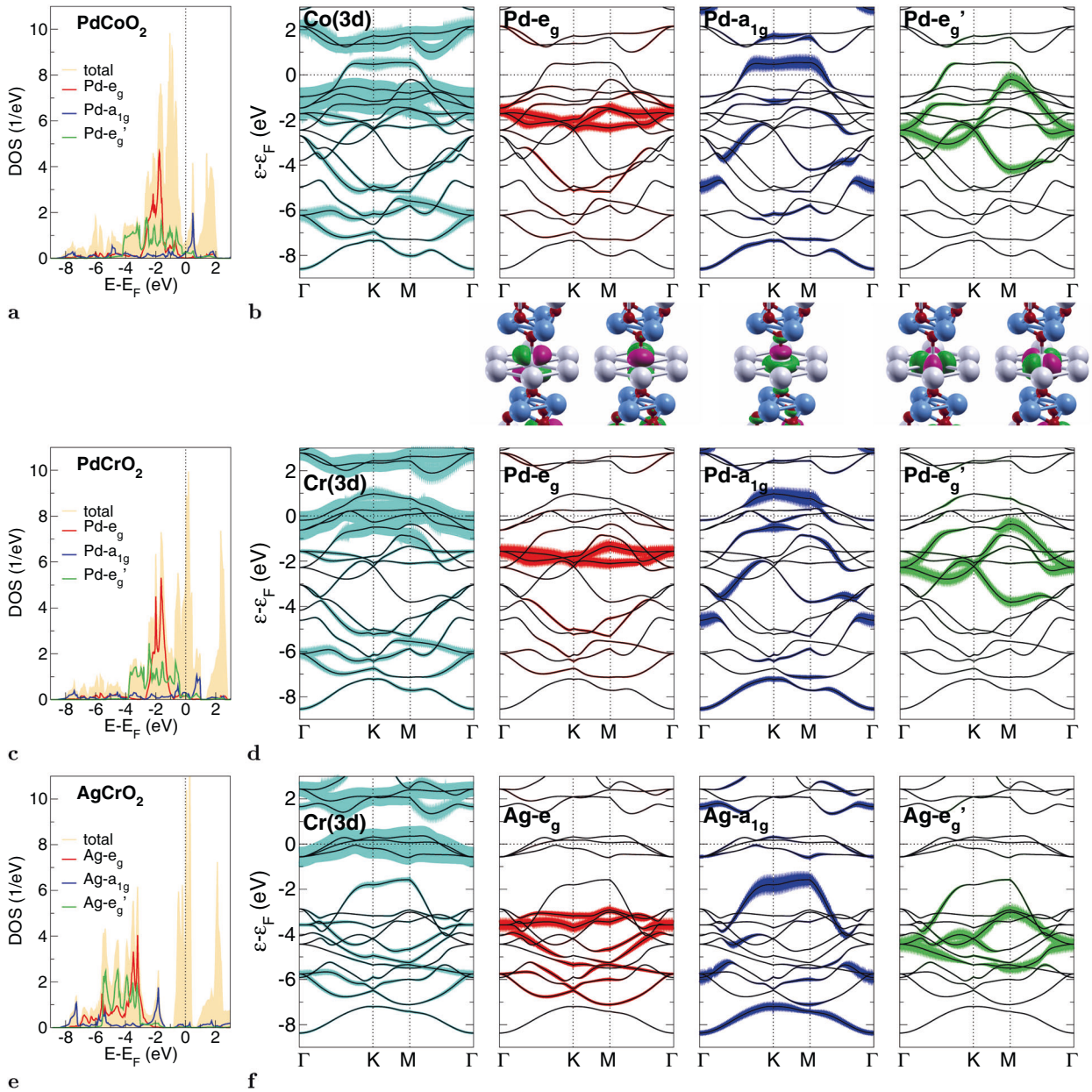

Fig. 3 DFT electronic structure of $PdCoO_2$, $PdCrO_2$ and $AgCrO_2$. a Total and orbital-resolved $\mathcal{A}$-site(4*d*) density of states. (**b**) Band structure along high symmetry lines in the $k_z = 0$ plane, with fatbands marking the $\mathcal{B}$-site(3*d*) and the orbital-resolved $\mathcal{A}$-site(4*d*) character. Additonally, the corresponding real-space Pd(4*d*) projected local orbitals are provided for the case of $PdCoO_2$: Pd (grey), Cr (lightblue) and O (red). **c**, **d** Same as (**a**, **b**) but for $PdCrO_2$. **e**, **f** Same as (**a**, **b**) but for $AgCrO_2$.

hints for localized Cr^{3+} $S = 3/2$ spins[12,71,73]. The QP peak at low energy is of dominant Pd(4*d*) character, therefore confirming the previously announced mechanism of a correlation-induced shift of a DFT-original deeper lying Pd-dominated band towards ε_F. The projected $AgCrO_2$ spectrum shows again the Mott-insulating Cr (3*d*) part along with the band-insulating Ag(4*d*) part. The plots of $A_\nu(\omega)$ render obvious that for $PdCoO_2$ the low-energy QP is for the most part constituted from a single Pd-dominated Bloch dispersion, which we call LE-Pd. The same holds for the $PdCrO_2$ case. Yet importantly, both QP peaks display the hybridizing contribution of Co/Cr-dominated functions, and the LE-Pd function moreover exhibts significant energy dependence. Both features point to the relevance of the subtle impact of electronic correlation onto the low-energy regime. Or in other words, the 'single-band' dispersion crossing ε_F, though not dominated by the strongly-interacting $\mathcal{B}$-site 3*d* orbitals, still carries subtle effects of correlations which most certainly rule (parts of) the challenging delafossite physics. But be aware of our difference in nomenclature; 'cPd' denotes the complete single low-energy dispersion, while 'LE-Pd' marks the most dominant A_ν contribution to it. The corresponding A_ν plot for $AgCrO_2$ shows that the band-insulating character part is equally dominated by a single LE-Ag dispersion, with the Mott-insulating character part once again carried by Cr(3*d*).

Finally note that the O(2*p*) states are mostly aligned with Ag(4*d*) in $AgCrO_2$, whereas they are located significantly deeper in energy than Pd(4*d*) in $PdCoO_2$ and $PdCrO_2$. Since there are no strong charge-transfer effects expected from t_{2g}-based Co,Cr(3*d*), the present treatment of excluding explicit Coulomb interactions within O(2*p*) should be reliable. There might be however scenarios, e.g., the hole doping of $AgCrO_2$, where O(2*p*)-based interaction effects could become non-negligible in delafossites.

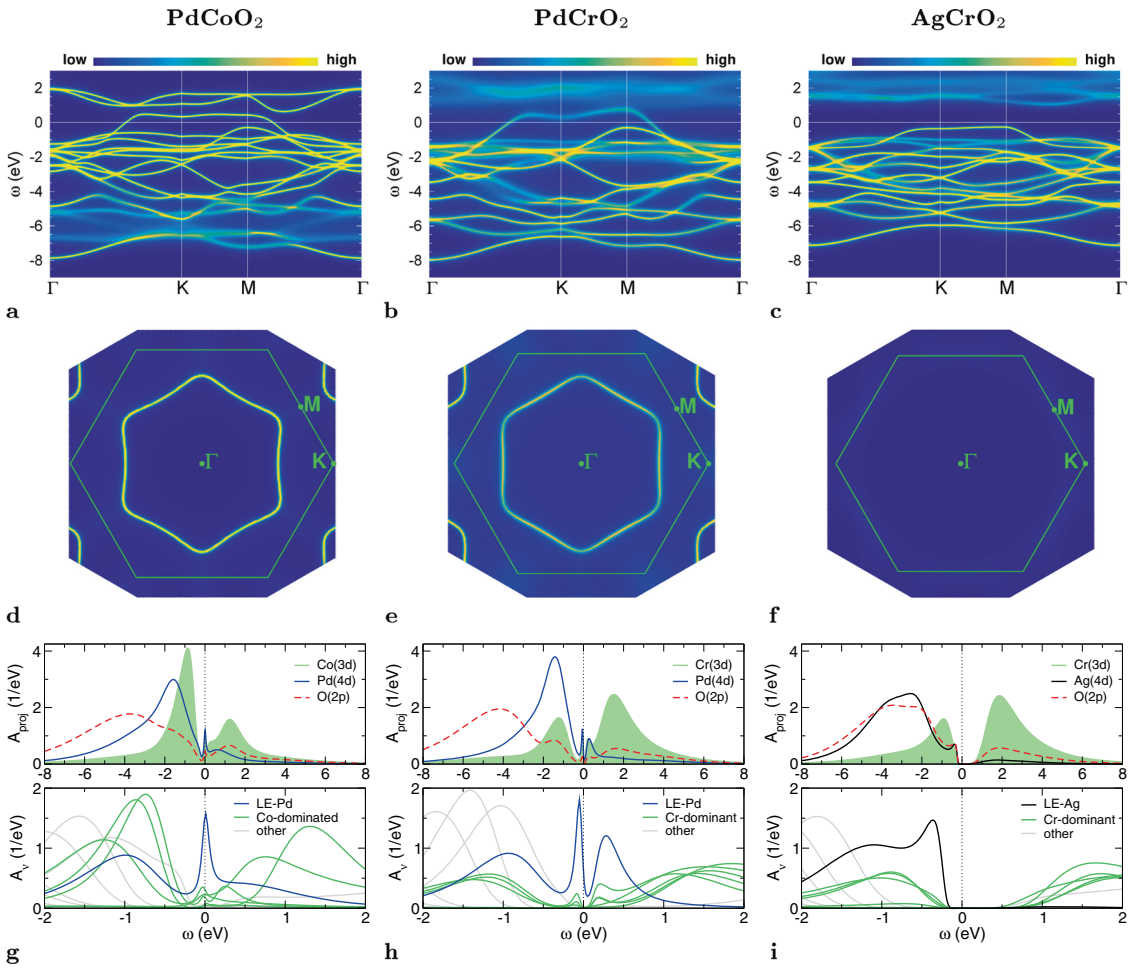

Fig. 4 Spectral properties of $PdCoO_2$, $PdCrO_2$ and $AgCrO_2$ according to paramagnetic DFT+DMFT. a–c k-resolved spectral function $A(\mathbf{k}, \omega)$ along high symmetry lines in the $k_z = 0$ plane. **d–f** Interacting Fermi surface in the $k_z = 0$ plane. **g–i** Site- and orbital-projected spectral function $A_{\mathrm{proj}}(\omega)$ (top) and Bloch-resolved spectral function $A_{\mathrm{v}}(\omega)$ (bottom), see text, respectively.

Extensions of conventional DFT+DMFT, e.g., as described in Ref. [74], are available to treat such effects.

After this overview, we want in the following discuss and comment on relevant underlying electron correlation aspects. First, the atomic-like picture of a fully-closed Co-t_{2g} subshell in the $PdCoO_2$ compound is of course an idealization. The DFT+DMFT occupancies per single orbital on Co at room temperature amount to $\{n_{e'_g}, n_{a_{1g}}\} = \{1.90, 1.93\}$, thus there is still about 4% local t_{2g} doping. The associated charge fluctuations together with the hybridizations on the low-energy QP dispersion point to a subtle connection between the Pd layer and the CoO_2 layer. This is underlined by the spectral comparison shown in Fig. 5, where one may observe that the ε_F-slope of the cPd dispersion, which is proportional to the Fermi velocity, has slightly increased with correlations. Usually, strong local electronic correlations lead to a reduction of the QP Fermi velocity, associated with a bandwidth renormalization toward smaller values. Yet here, the explicit Coulomb interactions are active in the CoO_2 layer and the cPd dispersion with dominant Pd(4*d*) weight mainly originates from the 'non-interacting' Pd layer. Seemingly, an implicit nonlocal effect of correlation steepens the dispersion, at least on a proof-of-principle level. This could be a contributing factor to the high conductivity of $PdCoO_2$. Again, (local) correlation effects appear not decisive in $PdCoO_2$, but their role still deserves further exploration.

The impact of electronic correlations is obviously crucial for $PdCrO_2$. On a more formal level, interactions lead to a metal-to-metal

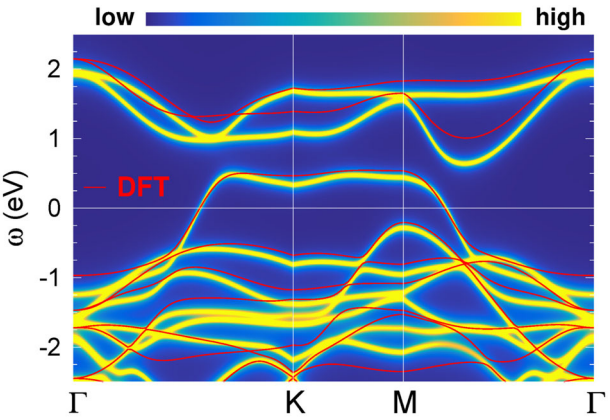

Fig. 5 k-resolved spectral function of $PdCoO_2$. Comparison between the DFT band structure (red) and the DFT+DMFT result.

transition between a system with Cr(3*d*)-dominated threefold dispersion at weak coupling and a system with Pd(4*d*)-dominated single dispersion at strong coupling. The question arises how this apparent quantum phase transition takes place with increasing interaction strength U. Figure 6a displays the spectral function and fatbands for the DFT limit ('$U = 0$') and for $U = 1.5$ eV, i.e., half the assumed correct interaction strength in $PdCrO_2$, in direct comparison. Of course, the $U = 0$ data is identical

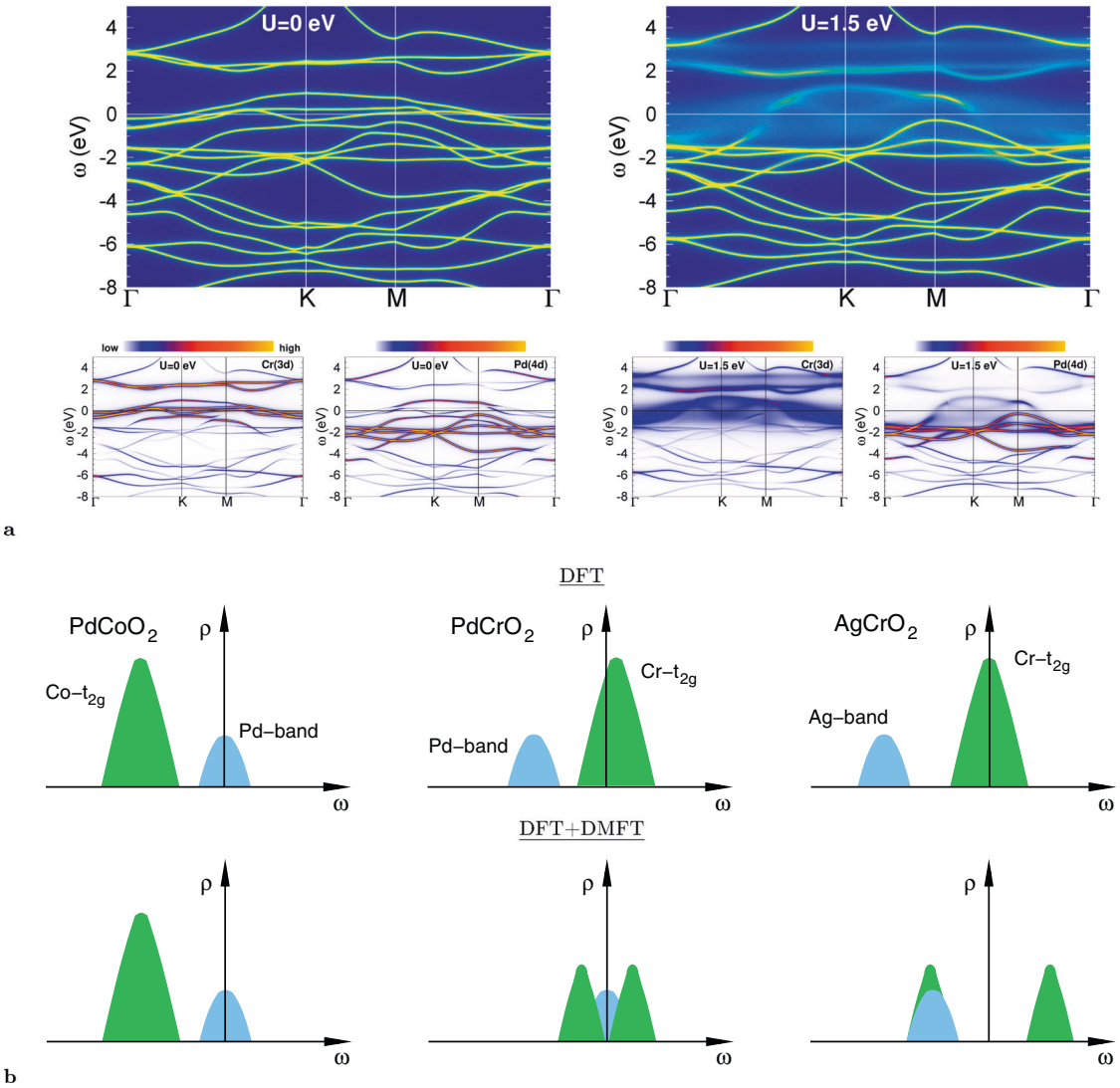

Fig. 6 On the correlation features in delafossites. a Spectral properties of $PdCrO_2$ for different interaction strengths. Left panel: $U = 0$ eV, i.e., DFT bands. Right panel: $U = 1.5$ eV. Top: spectral function, bottom: fatbands for Cr(3*d*) (left) and Pd(4*d*) (right) (from[72]). **b** Sketch of the basic differences in the **k**-integrated spectral function $\rho(\omega)$ for the most-relevant four bands close to the Fermi level among the studied delafossites. Top: DFT, bottom: DFT+DMFT. Left: $PdCoO_2$: Co-t_{2g} bands occupied, uppermost Pd(4*d*)-band half filled; middle: hidden-Mott $PdCrO_2$: Cr-t_{2g} bands 1/3 filled, uppermost Pd(4*d*)-band occupied; right: band-Mott insulating $AgCrO_2$: Cr-t_{2g} bands half filled, uppermost Ag(4*d*)-band occupied.

to what is shown in Fig. 3d, rendering the mechanism for the transition clear: The three bands at the Fermi level are filled with two electrons, and hence four electrons populate the altogether four bands when counting down in energy from ε_F. These four bands are of mixed Cr(3*d*), Pd(4*d*) character, with dominance from the 3*d* sector. Due to the given band entanglement, strong correlations transform three of them into Hubbard bands, and leave a resulting one with half filling at the Fermi level. Interestingly, for the intermediate coupling (right panel of Fig. 6a), the system adopts a 'strange' situation. The Cr-t_{2g} dispersions are very incoherent and not yet Mott localized, and the cPd dispersion is not yet fully established coherently. Note that especially the cPd dispersion, which appears weakly-interacting at strong and weak coupling, is intriguingly affected by correlations close to the given metal-to-metal transition. This underlines the intricate inter-layer physics that is at work in $PdCrO_2$ with its 'hidden-Mott' state. Note that in a pure model context, at least three bands would be necessary to capture a hidden-Mott scenario: one fully filled band and two bands with overall quarter filling when putting interactions to zero. Strong interactions should then transfer one electron from the filled band to both remaining bands, rendering them half-filled.

From a model perspective of correlated electrons, Kondo-lattice type of Hamiltonians describing strongly-interacting sites within a Fermi sea[75,76] has been discussed as a starting perspective for $PdCrO_2$[13]. Such a framework has then indeed put into practise in order to account for the coupling of the Cr spins to the Pd layer in the magnetically-ordered state[14]. However, as already mentioned in Ref. [13], a standard Kondo-lattice model of spins coupled to free electrons appears too simplistic to cover the full complexity of the above described hidden-Mott physics[77]. Modelling the electronic correlations that originate from the CrO_2 layer and spanning over to the Pd layer in a comprehensive way has most definitely to account for the outlined metal-to-metal transition.

Because of the $4d^{10}$ state of silver in $AgCrO_2$, an intricate band entanglement as in $PdCrO_2$ is missing. In the DFT limit, the three Cr-t_{2g} bands at the Fermi level are already half filled with three electrons. Thus the internal Mott transition in the CrO_2 layers does

not lead to a metal-to-metal transition, but to a more ordinary metal-to-insulator transition with increasing U. But there is a twist; the valence-band maximum of insulating $AgCrO_2$ is dominated by silver (and oxygen) character, highlighting the band-insulating aspect of the system. The compound is therefore best coined as band-Mott insulator.

To emphasize the key differences of the given delafossites from a minimal perspective, Fig. 6b summarizes the main features from the noted four-band perspective of $\mathcal{B}$-site derived t_{2g} bands and $\mathcal{A}$-site derived uppermost 4d band part.

MOTT DESIGN OF CORRELATED DELAFOSSITES

General considerations

We have seen in the previous section that in an interacting many-body sense, the revealed correlation effects in $PdCoO_2$ and $AgCrO_2$ are apparently not yet of particular breathtaking kind. The former compound is a straightforward metal with, from the current viewpoint, weak impact of correlations. The latter compound harbors strong correlations and is a combined band-Mott insulator, yet a Mott-insulating state per se is not a spectacular state of matter. On the other hand, the $PdCrO_2$ compound seems quite exotic with its entanglement between metallic and Mott-insulating characteristics. However, in the equilibrium state, $PdCrO_2$ behaves like an ordinary metal, even across the Néel temperature and in the ordered AFM phase[73]. The hidden-Mott state in the system is seemingly behaving like a 'sleeping dragon'. For its awakening and the display of more exciting physics, one has to drive the compound 'out of its comfort zone' by disturbance and further design.

Hence in the following subsections the focus will be on possible theoretical ways how to 'wake up the dragon' and to create new correlation phenomenology out of the intriguing scenario found in $PdCrO_2$. We will here only briefly comment on point-defect and pressure/strain effects in the next subsection, and afterwards will discuss in some more detail the effects of heterostructuring. An overview on recent experimental activities towards engineering correlated delafossites will close this section.

Defect engineering, pressure, and strain

Chemical doping either iso-valent or of charge-doping kind is a traditional route to modify a given electronic structure. The hole- and electron doping of cuprates by substitutional impurities which transfers a stoichiometric Mott insulator into a high-T_c superconductor represents the most famous example[78]. Melting the instrinsic Mott insulator in $PdCrO_2$ by defect-induced charge doping becomes indeed possible from supercell DFT+DMFT calculations in a corresponding dense-defect regime with symmetry breakings due to point defects. On the other hand, minor charge doping on the Cr site performed in a virtual-crystal approximation leads to a transfer of doping charge from the CrO_2 layers to the Pd layers, thus doping mainly the metallic band. We refer the reader to Ref. [13] for further details.

Additionally, iso-valent chemical doping may be promising from the metal-to-metal transition viewpoint given above. Namely, introducing e.g., Mo impurities on the Cr sublattice should lead to a reduction of the effective U in the d-shell on the $\mathcal{B}$ site, enabling access to the intriguing intermediate-coupling regime.

Application of pressure or strain can also result in a relevant change of the electronic structure. For instance, uniaxial pressure/strain along the c-axis would modify the Pd and CrO_2 layer separation, which may effect the band entanglement and the hidden-Mott physics. There is the possibility of driving the discussed metal-to-metal transition by metallizing the CrO_2 planes via applied pressure.

Out-of-plane $PdCrO_2$-$AgCrO_2$ heterostructures: correlated semimetallic states

As noted in the Introduction and hopefully became clearer in the previous sections, delafossites may be viewed as natural heterostructures with different electronic characteristics in the $\mathcal{A}$- and $\mathcal{B}O_2$-layers. It may be therefore obvious that a merging of delafossite physics and the ever-growing field of oxide heterostructures (see e.g., Refs. [79,80] for reviews) could turn out as a frutiful combination.

In fact, heterostructures from combining $PdCrO_2$ and $AgCrO_2$ may be of particular interest. Both compounds have similar lattice parameters, resulting in a minor mismatch, and differ only by one electron in the $\mathcal{A}$-site valence. However, their electronic phenomenology, i.e., hidden-Mott metal vs. band-Mott insulator, is quite different. Heterostructuring both delafossites provides therefore a specific doping scenario: by keeping the local environment rather undisturbed, filling modifications in the Cr-t_{2g} manifold (i.e., green spectra in middle and right part of Fig. 6b) inbetween the DFT values may be triggered. In the following we denote the DFT filling fraction of the Cr-t_{2g} states by a. Then the given heterostructures formally interpolate directly between the hidden-Mott metal ($a = 1/3$) and the band-Mott insulator ($a = 1/2$), and should show via which path both phases are connected.

Alternate stackings of Pd, CrO_2 and Ag layers, i.e., straightforward out-of-plane heterostructures, are a natural realization of such a scenario. Note that a 'simple' interface construction between wide blocks of $PdCrO_2$ and $AgCrO_2$ might not be an ideal research object, since presumably, most of the interface modifications to transport would be masked by the metallic $PdCrO_2$ block. However, another type of heterostructure may also be promising, namely an in-plane variation within the $\mathcal{A}$ layer from intermixing the Pd and Ag content in an ordered fashion. This type should not be immediately linked to the doping scenario described above, because of the inherent change of the $\mathcal{A}$-layer character. But it could benefit from the specific delafossite layer (dis)entangling, and possibly give rise to different scenarios of a designed 2D lattice within a Mott background.

Three heterostructures with different $PdCrO_2/AgCrO_2$ stacking along the c-axis are designed, namely $Pd_{2/3}Ag_{1/3}CrO_2$, $Pd_{1/2}Ag_{1/2}CrO_2$, and $Pd_{1/3}Ag_{2/3}CrO_2$ (see Fig. 7). The lattice parameters are chosen from linear-interpolating the respective experimental data of the bulk structures (cf. Table 1), and the Hubbard U (identical on every Cr site) is also correspondingly interpolated from the limiting delafossite cases (see Ref. [72] for further details).

Before discussing the numerical results, let us briefly brainstorm about the electronic structure condition. From the $PdCrO_2$ perspective, the additional blocking layers of Ag kind as well as the stronger Mott-insulating character induced therefrom into the CrO_2 layers should increase correlations within the Pd layers, too. But this will again happen in a more subtle way than in standard correlated systems, where an associated Coulomb repulsion for such a layer is increased when looking for stronger correlation effects. Remember that there is no Hubbard U on Pd and all correlation increase has to take place in a nonlocal way from the surrounding layers. Thus, the present heterostructures pose a quite original correlation problem at low energy; a half-filled Pd layer without intra-layer interaction, subject to rising 'Coulomb pressure and confinement' imposed from the neighboring layers. How does the single electron of dominant Pd(4d) character cope with that situation?

Figure 8 displays the summarized DFT+DMFT spectral properties at room temperature for the three heterostructures. A detailed discussion, also concerning stability issues and with extension to lower-temperature properties, can be found in Ref. [72]. The main result, common to all structural cases, may be extracted from the low-energy comparison of the **k**-resolved and the **k**-integrated data: while there are still QP-like dispersions visible in $A(\mathbf{k}, \omega)$ at

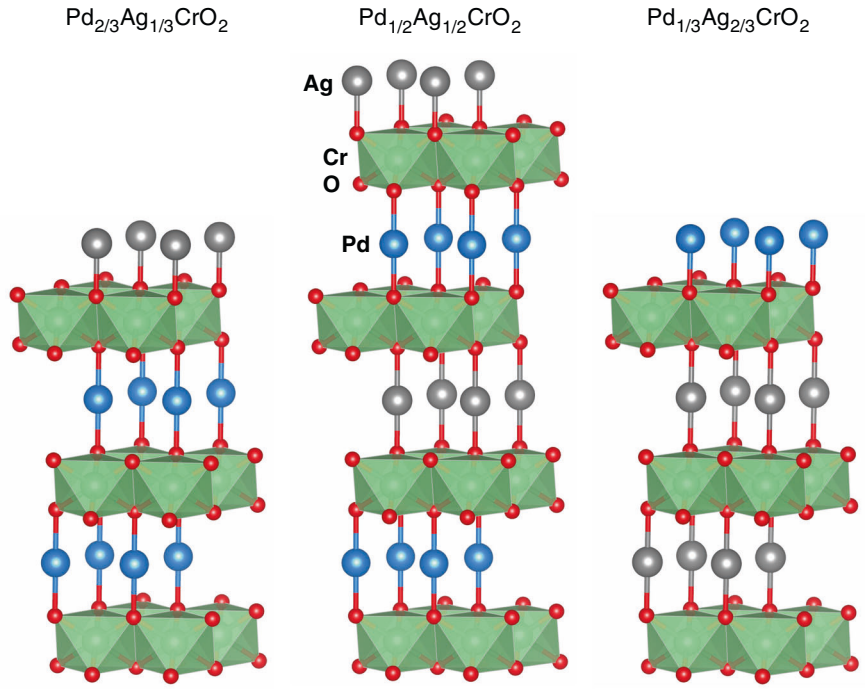

Fig. 7 Crystal structures of the designed out-of-plane heterostructures. $Pd_{2/3}Ag_{1/3}CrO_2$, $Pd_{1/2}Ag_{1/2}CrO_2$ and $Pd_{1/3}Ag_{2/3}CrO_2$ (from left to right) result from different stackings along the *c*-axis. Pd: blue, Ag: grey, Cr: green and O: red. From Ref. [72].

the Fermi level, the integrated spectra shows vanishing spectral weight at ε_F. We coin this puzzling electronic state as correlation-induced semimetal (CIS), which is obviously a result of the intriguing correlation scenario described above. Upon rising obstruction of transport, the key Pd(4*d*) electron can neither localize in real space (as in a Mott insulator) nor rest in a filled band (as in a band insulator). Hence it reduces the low-energy spectral weight as much as possible for an intact half-filled band, resulting in the CIS state. Note that this finding is not an artifact of the analytical continuation from Matsubara space to real frequencies, as the result is confirmed from both, maximum-entropy as well as Padé methods[72]. In some sense it amounts to a very strong reduction of the usual QP coherence scale of strongly correlated electrons, yet by still keeping the 'coherence' of the original dispersion. To our knowledge, such a rather exotic electronic state has not yet been reported in correlated matter and it awaits experimental verification.

Since the effective $\mathcal{A}$-site occupation is modified from the alternate-stacking architecture, the problem can also be pictured from an alternative viewpoint, namely from a formal change of the DFT filling factor a of Cr-t_{2g} (cf. Fig. 6b). The a values for the given heterostructures may formally be assigned by linear interpolation of the values for $PdCrO_2$ ($a = 1/3$) and $AgCrO_2$ ($a = 1/2$). Accordingly, the metallicity with respect to a is depicted in Fig. 8j. The transformation of the CIS states to the hidden-Mott state or the band-Mott insulator of the respective bulk compounds may be studied with different heterostructure layerings. It is very likely from Fig. 4i and Fig. 8i, that inbetween the CIS and the band-Mott insulator, there is another metallic regime. Notably, hole doping of the band-Mott-insulating state implements charge carrier into the more dominant band-insulating part of $AgCrO_2$. A doping $a > 1/2$ cannot be facilitated anymore by changing the $\mathcal{A}$-site TM(4*d*) ion, but modifying the $\mathcal{B}$-site TM(3*d*) might work. The regime $a < 1/3$ could in principle be reached by replacing Pd with Rh. But the Rh^+ ion with $4d^8$ configuration appears non-existing in known solid-state materials, and henceforth the stability of $RhCrO_2$ delafossite is very unlikely. Still in a Gedankenexperiment, since also instructive for the understanding of the hidden-Mott state, we performed calculations for hypothetical $RhCrO_2$, using the lattice parameters and Hubbard U of $PdCrO_2$. The results are shown in Fig. 9. The DFT band structure at lower energy exhibits the expected upward shiftings of the dispersions compared to the Pd compound. The filling of the Cr-t_{2g} dominated bands is hence smaller, close to unity (i.e., $a \sim 1/6$). Surprisingly, interactions still establish a near hidden-Mott state with a half-filled Cr-t_{2g} subshell. This underlines the significant coupling between the $\mathcal{A}$ layer and the CrO_2 planes. The fermiology becomes twofold in the Rh compound, associated with a shrinking of the original warped hexagonal sheet and the appearance of novel hole sheets around M (periodically arranged in a sixfold way). Note that Γ- and M-sheet nearly touch in a Dirac-like crossing along Γ-M. The appearance of the M-sheet is not that surprising, since the corresponding dispersion with the maximum at M is observed just below the Fermi level in $PdCrO_2$ (cf. Fig. 4b). Finally, the two-band picture is completed by observing two dominant LE-Rh contributions $A_\nu(\omega)$ close to ε_F. Furthermore, Fig. 9d displays that the Cr-t_{2g} dominated dispersions are not completely transformed into Hubbard bands by interactions, but show reduced weight at the Fermi level. In conclusion, if existing, $RhCrO_2$ would be a two-band metal with even stronger entangling between Cr(3*d*) and TM(4*d*). Reaching such a two-band regime in metallic delafossite, possibly by different doping/engineering routes of $PdCrO_2$, would be highly interesting.

In-plane alternations of $PdCrO_2$-$AgCrO_2$ type: Dirac(-like) states and emergent flat-band physics

Finally, let us push the limits of conceivable delafossite engineering even somewhat further, by interpreting the metallic implication of Pd in $PdCrO_2$ and the band-insulating implication of Ag in $AgCrO_2$ theoretically footlose. Instead of engineering $PdCrO_2$ 'out of plane' from replacing Pd layers by Ag layers, one may imagine an 'in-plane' alternation from replacing Pd sites by Ag sites in the periodically-repeated $\mathcal{A}$ layer. As a result, a novel natural-heterostructure delafossite emerges, but now with a decorated

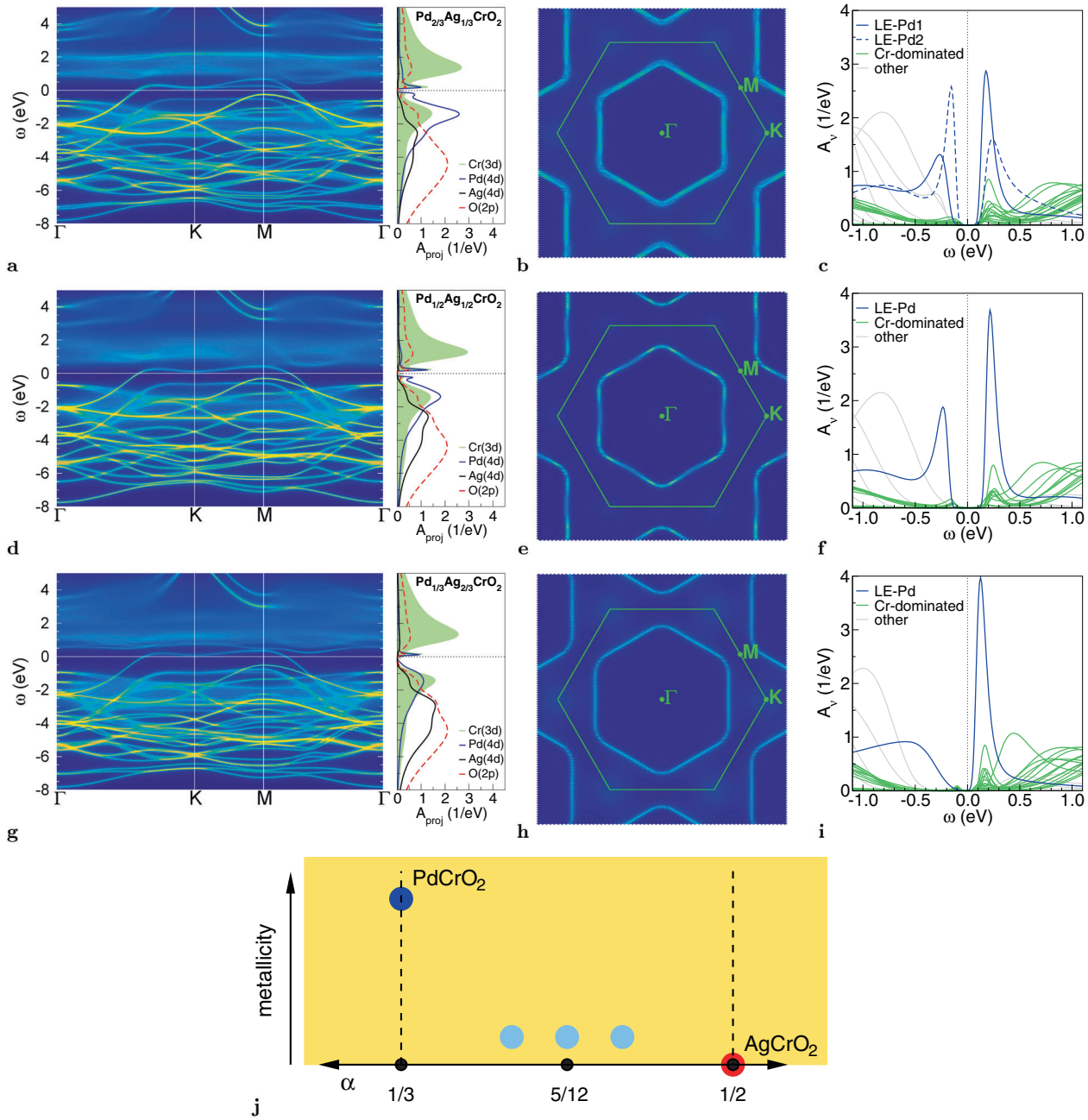

Fig. 8 Paramagnetic DFT+DMFT spectral data for the out-of-plane heterostructures. a–c $Pd_{2/3}Ag_{1/3}CrO_2$, **d–f** $Pd_{1/2}Ag_{1/2}CrO_2$ and **g–i** $Pd_{1/3}Ag_{2/3}CrO_2$. **a**, **d**, **g** Spectral function $A(\mathbf{k}, \omega)$ along high-symmetry lines in the $k_z = 0$ plane of reciprocal space (left) and **k**-integrated site- and orbital-projected spectral function (right). **b**, **e**, **h** Fermi surface for $k_z = 0$ within the first Brillouin zone (green hexagon). **c**, **f**, **i** **k**-integrated Bloch contribution $A_\nu(\omega)$ with characterization of dominance. From Ref. [72]. **j** Schematic resulting room-temperature metallicity with respect to the DFT filling factor α of the Cr-t_{2g} bands. Blue: metal $PdCrO_2$, red: band-Mott insulator $AgCrO_2$, and lightblue: CIS $Pd_{2/3}Ag_{1/3}CrO_2$, $Pd_{1/2}Ag_{1/2}CrO_2$ and $Pd_{1/3}Ag_{2/3}CrO_2$ (from left to right).

$\mathcal{A}$ layer. The viewpoint behind arises from picturing the $\mathcal{A}$ layer in hidden-Mott delafossite as a canonical single-band triangular lattice at half filling, embedded in a Mott-insulating background. By manipulating the features of this triangular lattice, a platform for studying correlation effects in such a Mott background may be generated. The simplest manipulations in this regard are given by the straightforward transformations of the original triangular lattice via the K- and M-point ordering instabilities, associated with the honeycomb (K) and the kagomé (M) lattice (see Fig. 10a). Realizing those lattices within a Mott background is exciting because they host Dirac-semimetallic and in the case of the kagomé lattice additionally flat-band dispersions. The study of these dispersion features under the possible influence of strong correlations is a recent emerging research field in condensed matter, see e.g., Refs. [81–83].

To facilitate this reductions of the triangular lattice, the introduction of periodic blocking sites which ideally disconnect hopping processes, can be a promising route. This concept has been e.g., used to account for the effect of charge ordering onto transport properties in Na_xCoO_2[84,85]. From the nominal Ag(4*d*) filled-shell in the CrO_2-based delafossites, we assume in the present context that Ag sites within the Pd layer may serve as such blocking sites. For sure, finite

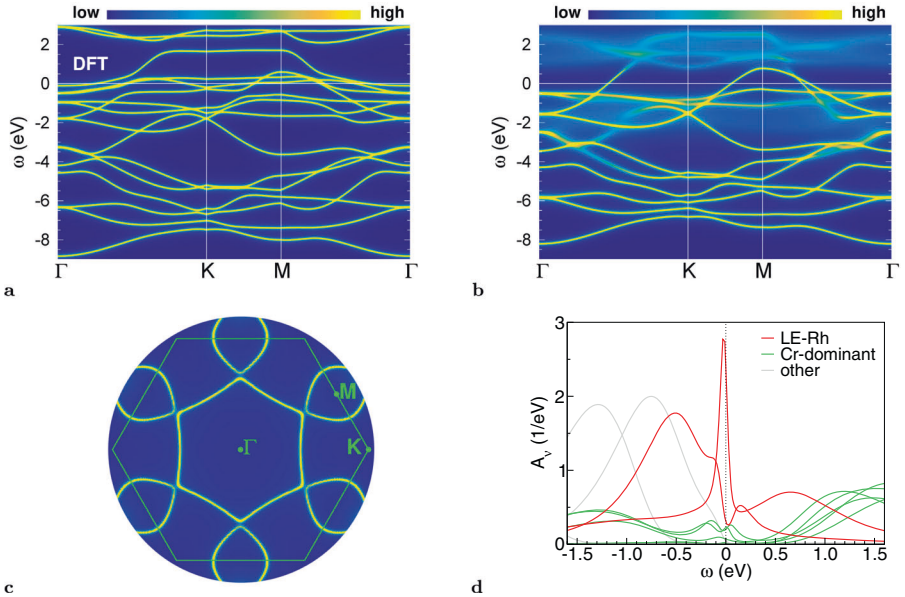

Fig. 9 Spectral properties of hypothetical $RhCrO_2$. a DFT band structure, **b**–**d** DFT+DMFT features: **b** spectral function $A(\mathbf{k}, \omega)$, **c** Fermi surface and **d** **k**-integrated Bloch contribution $A_\nu(\omega)$ with characterization of dominance.

covalency will only realize a partial blocking, however, this may still be sufficient to mimic basic honeycomb- or kagomé-lattice features. To realize a honeycomb(kagomé) lattice in that spirit within the $\mathcal{A}$ layer, one out of three(four) in-plane Pd sites has to be replaced by Ag. Note that though preparing such orderings in the lab will be surely demanding, a layer-by-layer growth might still be feasible from tailoring the layer stoichiometry. If the given Pd-Ag in-plane orderings are thermodynamically stable (for given temperature, pressure, strain, etc.), nature will take its course in realizing the periodic effective honeycomb/kagomé pattern. For the honeycomb case, Fig. 10b depicts the designed delafossite structure. The DFT+DMFT calculations for both effective-lattice systems are again performed with corresponding linear interpolation of the known lattice parameters and the chosen Hubbard U values for the bulk compounds. The honeycomb(kagomé) structure asks for a supercell of three(four) original formula units. Note that we utilitzed a somewhat lower system temperature of $T = 193$ K for both structural cases, since from general inspection of the spectral properties, the coherence scale for stable quasiparticles appears smaller for the given in-plane alternations compared to the out-of-plane heterostructures.

In Fig. 10 we first show the spectral function of the effective honeycomb structure. From graphene studies it is well known that the nearest-neighbor (NN) tight-binding electronic structure of the half-filled honeycomb lattice is semimetallic, with prominent Dirac dispersions (i.e., massless Dirac fermions) at the K point in reciprocal space[86]. The low-energy spectrum of the present effective lattice in the delafossite setting shows indeed some resemblance of this feature. First, the CrO_2 planes remain Mott-insulating upon the in-plane (Pd,Ag) structuring and there are two Pd-dominated dispersion close to ε_F (see Fig. 10a). A Dirac-like dispersion around K is indicated, yet shifted, with different filling and different overall dispersion compared to graphene. Still, some blocking behavior of Ag is realized, transforming the original $PdCrO_2$ low-energy dispersion in direction towards the canonical honeycomb dispersion. The site-orbital content in Fig. 10b renders obvious that Ag(4*d*) and Cr(3*d*) have quite a weight on the twofold dispersion around the Fermi level, highlighting the entangled nature. Note that there are two symmetry-inequivalent Cr positions, with Cr′ mirroring the position of the blocking site within the Cr sublattice.

The NN tight-binding electronic structure of the kagomé lattice is known for its flat-band feature at one side of the band edge, as well as for the Dirac dispersion at 4/3(2/3) filling depending of the sign of the NN hopping[81]. In the present case, the flat-band feature should appear at the upper band edge and thus the Dirac point at 2/3 filling. Figure 11 depicts the resulting spectral function of effective-kagomé (Pd,Ag)CrO_2, and from a brief look the canonical kagomé features are hard to decypher. The intriguing effect of correlations and only-partial Ag blocking render things difficult to read. Yet after a closer look, and after also comparing with the non-interacting DFT states, the remains of the flat-band feature can be located around 1 eV above the Fermi level. Interestingly, the interactions in the delafossite structure seemingly transfer spectral weight from there towards ε_F. Close to Γ, a waterfall-like spectral signature may be observed. Hence a flat, but at $T = 193$ K rather incoherent, low-energy feature ranging from K to M and halfways to Γ emerges (see Fig. 11a). Its spectral content is dominated by the symmetry-equivalent subclass Pd″(4*d*), which collects two out of the three in-plane Pd sites of the supercell. But again, contribution from once more formally Mott-insulating Cr (3*d*) is not negligible. The Dirac-dispersion feature at K from the canonical kagomé lattice can also be identified at about −0.6 eV. Thus albeit again the finite covalency of in-plane Ag does not allow for complete blockings, and also the original half-filled nature of the Pd layer in $PdCrO_2$ is disturbed by introducing Ag, the interplay of the hidden-Mott physics with model-kagomé features gives rise to interesting low-energy behavior.

In conclusion, expectedly neither the effective-honeycomb nor the effective-kagomé lattice realization in the modifed $PdCrO_2$ structure enables canonical textbook dispersions at the Fermi level. But as a proof of principles, the in-plane engineering of delafossites may be a route to create nontrivial low-energy dispersions which are subject to the puzzling layer-entangled correlation delafossite physics.

Experimental work on engineering correlated delafossites

After discussing some theoretical designing ideas, we eventually take a quick look on the current status of designing and manipulating correlated delafossites in experiment.

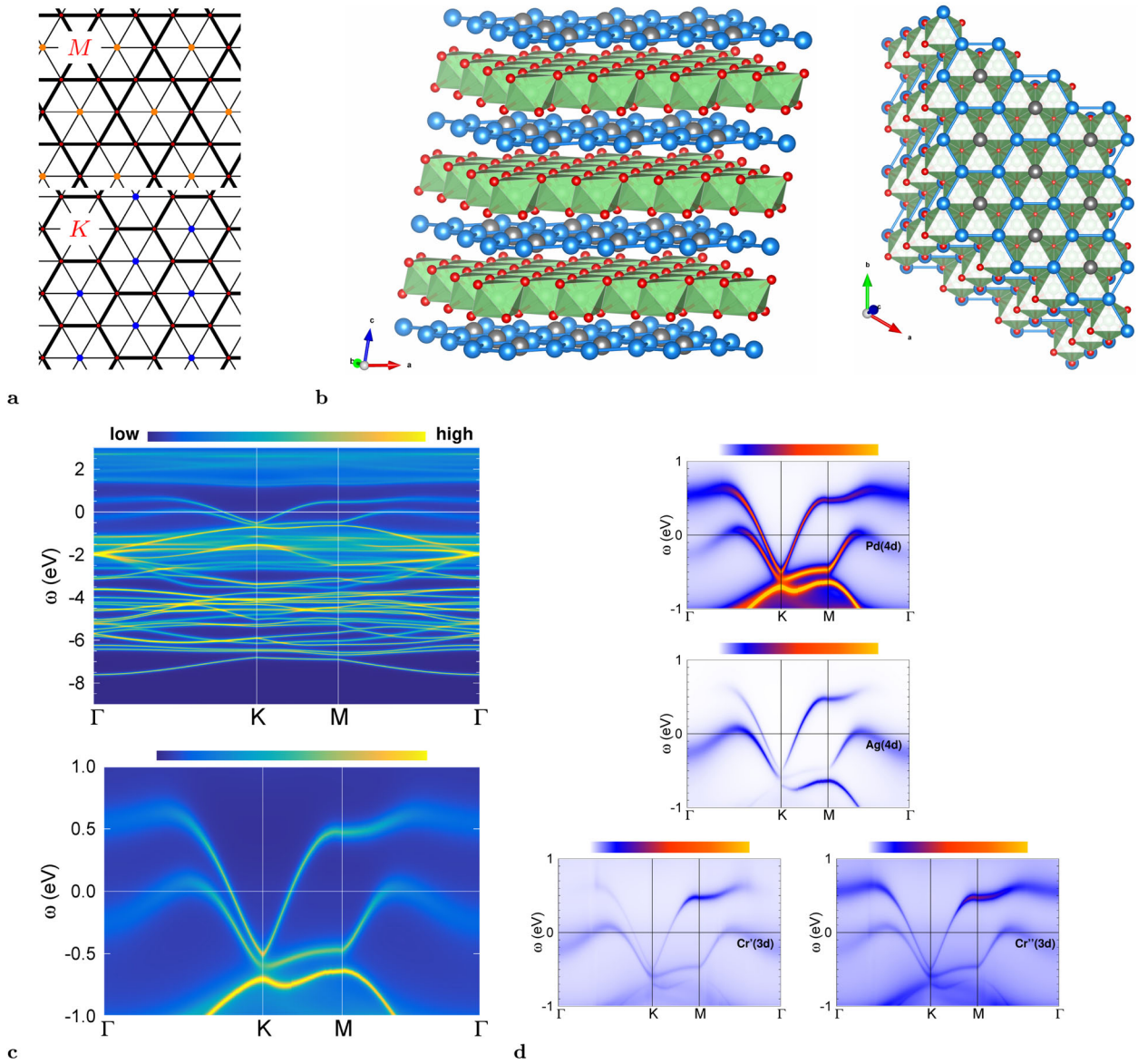

Fig. 10 Effective-honeycomb (Pd,Ag)CrO_2 delafossite. a In-plane design of the $\mathcal{A}$ layer via the natural triangular-lattice ordering instabilities of K-point (honeycomb) and M-point (kagomé) kind (from[109]). **b** Designed crystal structure from understanding Pd(Ag) positions as active (blocking) sites; Pd: blue, Ag: grey, O: red; Cr: green. Left: 3D view and right: view onto the effective honeycomb lattice of Pd sites. **c**, **d** Interacting spectral information from DFT+DMFT at $T = 193$ K. (**c**) Spectral function in (top) larger and (bottom) smaller energy window. **d** Orbital-site content ('fatbands'), from top to bottom: Pd(4*d*), Ag(4*d*) as well as both symmetry-inequivalent Cr(3*d*), i.e., Cr'(3*d*) and Cr''(3*d*) (see text).

The preparation of bulk single crystals has been demanding for quite some years, but nowadays does not really pose a tough problem anymore for the known delafossites. They are nowadays even used as electrocatalyst for hydrogen evolution reactions[87]. However, layer-by-layer growth from e.g., pulsed-laser deposition (PLD) or molecular-beam epitaxy (MBE), especially for the metallic systems, remained challenging until recently. But starting from about two years ago, the number of successful reports on grown metallic delafossites is increasing. For instance, thin-film preparation of $PdCoO_2$[88–91] and $PdCrO_2$[92,93] has been reported by several groups. The transport properties of such films share in most cases the exceptional high conductivity known from the bulk compounds, and device-oriented ideas have been proposed[94]. Notably, in the ultra-thin limit of $PdCrO_2$ films grown on a single-layer of $CuCrO_2$, a significant increase of resistivity is reported[92].

Recent surface-sensitive studies on metallic delafossites are furthermore promising in revealing details on the impact of correlations. Strong Rashba-like spin splitting in CoO_2 and RhO_2 related delafossite surface states[95] and itinerant ferromagnetism on the Pd-terminated (polar) surface of $PdCoO_2$[96,97] have been observed.

Chemical doping and/or introduction of reasonable amounts of point defects through irradiation appears quite difficult in metallic delafossites[98]. Systematic studies on substitutional doping are very rare[99]. Apparently, the high-purity crystal state of these materials[11] renders it on the other hand hard to implant a sizable amounts of point defects.

Nonetheless, the research activity on (metallic/correlated) delafossites is high and expected to further increase. Experimental investigations on specifically designed delafossites, e.g., along the lines of the theoretical propositions discussed in the previous section, are believed to become available soon.

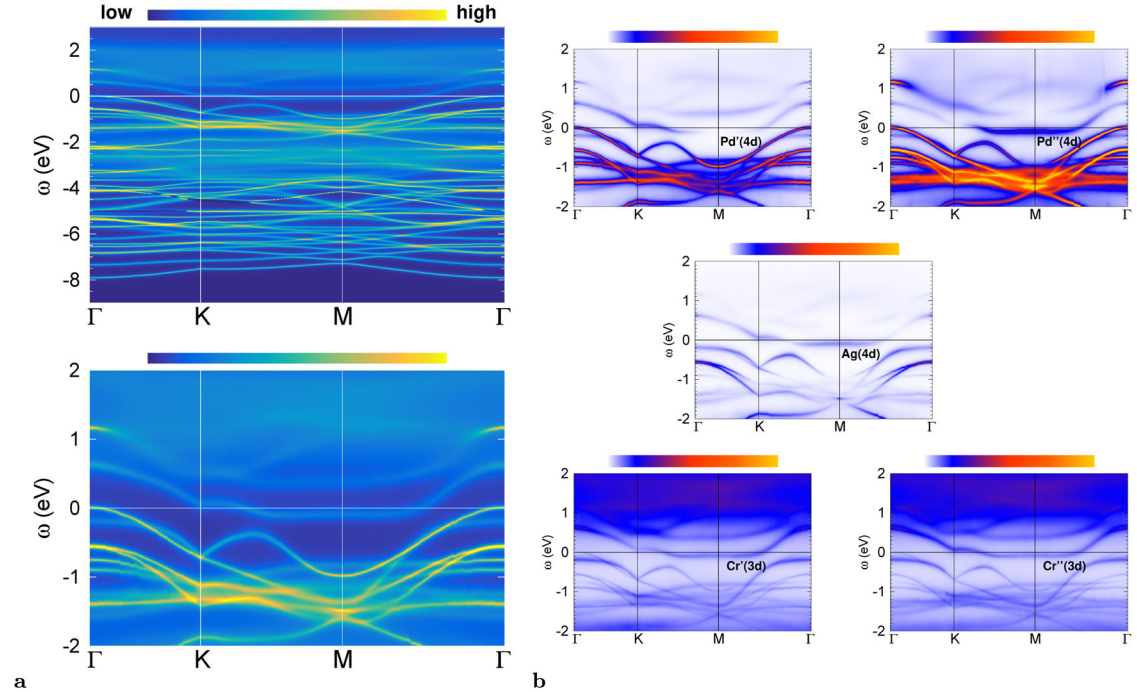

Fig. 11 Interacting spectral information for effective-kagomé (Pd,Ag)CrO_2 from DFT+DMFT. a Spectral function in (top) larger and (bottom) smaller energy window. **b** Orbital-site content ('fatbands'), from top to bottom: both symmetry-inequivalent Pd(4*d*), i.e., Pd'(4*d*) and Pd''(4*d*), Ag(4*d*) as well as both symmetry-inequivalent Cr(3*d*), i.e., Cr'(3*d*) and Cr''(3*d*) (see text). All data for $T = 193$ K.

CONCLUSIONS AND OUTLOOK

Delafossites are not new materials in condensed matter physics. They have been around for quite some time and also strong correlation phenomena have been discussed e.g., in the context of insulating Cu-based compounds within the early days of high-T_c cuprate research. Yet the concise studies of high-purity metallic delafossites that started about ten years ago brought them (back) into the spotlight of condensed matter research. Though known as the best-conducting oxides, they still share the inherent property of hosting strongly correlated electrons common to most transition-metal oxides. But whereas in standard Mott materials such as e.g., V_2O_3, $YTiO_3$ or La_2CuO_4 the competition between Coulomb repulsion and itinerancy establishes an overall Mott-insulating state (or a metal-insulator transition with temperature), electron correlations in delafossites act much more subtle and their characteristics can be quite elusive. In the extreme limit of CrO_2-based delafossites, they can give rise to layer-selective Mottness which is then coupled to the remaining metallic and/or band-insulating layers in an unusual way.

What makes delafossites so different from other oxides? The dumbbell-bond separation between the $\mathcal{A}$ and $\mathcal{B}O_2$ layers leaves them rather 'freestanding', which enables a seemingly independent electronic behavior. As a result, the scattering within the $\mathcal{A}$ layer and from there with the $\mathcal{B}O_2$ layers is surprisingly small, for reasons which very details still need further exploration. Notwithstanding, a delicate coupling between both layer types prevails, as e.g., displayed by the here presented results of the correlation-induced increase of Fermi velocity in $PdCoO_2$ and the metal-to-metal transition with increasing U in hidden-Mott $PdCrO_2$. In the general correlation context, the latter compound stands out and is undoubtly the most 'enigmatic' delafossite. But in standard measurements of transport and spectroscopic behavior, there are (yet) no dramatic signs of its unusual correlated nature. The recent photoemission study of Sunko et al.[14], which speculates about spin-charge separation in $PdCrO_2$, appears as an important experimental step to face its correlated phenomenology. Albeit driving the system out of its 'comfort zone' seems necessary to unravel more facets of correlated electrons in $PdCrO_2$.

Let us emphasize once more that the present review deals with a selective materials view on correlation effects in delafossites. There are various further members of this oxide family that deserve attention in this respect. For instance, the $AgNiO_2$ compound is known to show challenging charge and spin ordering[100], with possiblly increased relevance of Hund's coupling physics[101]. In view of magnetism, there is a broad literature on $PdCrO_2$ and related spin-active delafossites, e.g., Refs. [14,77,102–108], but in this short review we focussed on the paramagnetic correlation aspects. The magnetic properties are surely a relevant feature and based on correlations. However as often the case in TM oxides, those properties seem secondary once strong correlations have been established. For instance, the 120° ordering at lower temperature in $PdCrO_2$ and $AgCrO_2$ may only set in after the Mott-critical behavior with strong local $S = 3/2$ spin formation in the CrO_2 layers is realized. A deeper understanding of the underlying exchange mechanisms should therefore ask for a thorough account of the correlated-electron states. It might also be conceivable that explicit local Coulomb interactions on the $\mathcal{A}$ site prove necessary for describing the fine details of delafossite magnetism. It this regard, it is understood that the spin degree of freedom may be crucial to access the delafossite many-body physics by experimental means.

As we stressed several times, the design aspect comes in naturally when engaging oneself with delafossites. The bulk compounds are comparably simple in structure and there are various different delafossites ranging from metallic to insulating. Plus, they may host such intriguing phases as the hidden-Mott phase. Hence taking advantage of this potentially plethora of design possibilities is tempting and we tried to discuss some ideas in that direction in the present text. Besides magnetism, we also left out the aspect of topology. The latter is very prominent in modern condensed matter research, and could

also play a vital role in engineered delafossites. One may surely imagine architectures hosting nontrivial topological fermions within the layer-selective Mott background of strongly correlated delafossites. A first minimal step towards such scenarios has here been indicated by unveiling Dirac(-like) dispersions by design.

To conclude, albeit delafossites have not yet entered the biggest stage of condensed matter physics, they surely are a 'colorful' addition to the realm of correlated materials. It is hoped that this brief review stimulates further theoretical and experimental research in finding ways to unleash the so far mostly hidden nature of strong electronic correlations in delafossites.

DATA AVAILABILITY

All data are available from the corresponding author upon request.

CODE AVAILABLITY

The code used to perform the DFT+DMFT calculations is available upon reasonable request to the author.

Received: 12 January 2021; Accepted: 7 June 2021;
Published online: 23 July 2021

REFERENCES

1. Friedel, C. Sur une combinaison naturelle des oxydes de fer et de cuivre, et sur la reproduction de l'atacamite. *Compt. Rend. Acad. Sci. Paris* **77**, 211 (1873).
2. Rogers, A. F. Delafossite, a cuprous metaferrite from Bisbee, Arizona. *Amer. Jour. Sci.* **35**, 90 (1913).
3. Shannon, R. D., Rogers, D. B. & Prewitt, C. T. Chemistry of noble metal oxides. I. Syntheses and properties of ABO_2 delafossite compounds. *Inorg. Chem.* **10**, 713 (1971).
4. Prewitt, C. T., Shannon, R. D. & Rogers, D. B. Chemistry of noble metal oxides. II. Crystal structures of platinum cobalt dioxide, palladium cobalt dioxide, coppper iron dioxide, and silver iron dioxide. *Inorg. Chem.* **10**, 719 (1971).
5. Rogers, D. B., Shannon, R. D. & Prewitt, C. T. Chemistry of noble metal oxides. III. Electrical transport properties and crystal chemistry of ABO_2 compounds with the delafossite structure. *Inorg. Chem.* **10**, 723 (1971).
6. Anisimov, V. I., Poteryaev, A. I., Korotin, M. A., Anokhin, A. O. & Kotliar, G. First-principles calculations of the electronic structure and spectra of strongly correlated systems: dynamical mean-field theory. *J. Phys.: Condens. Matter* **9**, 7359 (1997).
7. Lichtenstein, A. I. & Katsnelson, M. I. Ab initio calculations of quasiparticle band structure in correlated systems: LDA++ approach. *Phys. Rev. B* **57**, 6884 (1998).
8. Kotliar, G. et al. Electronic structure calculations with dynamical mean-field theory. *Rev. Mod. Phys.* **78**, 865 (2006).
9. Kawazoe, H. et al. P-type electrical conduction in transparent thin films of $CuAlO_2$. *Nature* **389**, 939 (1997).
10. Daou, R., Frésard, R., Eyert, V., Hébert, S. & Maignan, A. Unconventional aspects of electronic transport in delafossite oxides. *Sci. Technol. Adv. Mater.* **18**, 919 (2017).
11. Mackenzie, A. P. The properties of ultrapure delafossite metals. *Rep. Prog. Phys.* **80**, 032501 (2017).
12. Noh, H.-J. Direct observation of localized spin antiferromagnetic transition in $PdCrO_2$ by angle-resolved photoemission spectroscopy. *Sci. Rep.* **4**, 3680 (2014).
13. Lechermann, F. Hidden Mott insulator in metallic $PdCrO_2$. *Phys. Rev. Mater.* **2**, 085004 (2018a).
14. Sunko, V. Probing spin correlations using angle-resolved photoemission in a coupled metallic/Mott insulator system. *Sci. Adv.* **6**, eaaz0611 (2020a).
15. Huda, M. N., Yan, Y., Walsh, A., Wei, S.-H. & Al-Jassim, M. M. Group-IIIA versus IIIB delafossites: electronic structure study. *Phys. Rev. B* **80**, 035205 (2009).
16. Seshadri, R., Felser, C., Thieme, K. & Tremel, W. Metal-metal bonding and metallic behavior in some ABO_2 delafossites. *Chem. Mater.* **10**, 2189 (1998).
17. Sheets, W. C. Silver delafossite oxides. *Inorg. Chem.* **47**, 2696 (2008).
18. Imada, M., Fujimori, A. & Tokura, Y. Metal-insulator transitions. *Rev. Mod. Phys.* **70**, 1039 (1998).
19. Zaanen, J., Sawatzky, G. A. & Allen, J. W. Band gaps and electronic structure of transition-metal compounds. *Phys. Rev. Lett.* **55**, 418 (1985).
20. Anisimov, V. I., Nekrasov, I. A., Kondakov, D. E., Rice, T. M. & Sigrist, M. Orbital-selective Mott-insulator transition in $Ca_{2-x}Sr_xRuO_4$. *Eur. Phys. J. B* **25**, 191 (2002).
21. Biermann, S., Poteryaev, A., Lichtenstein, A. I. & Georges, A. Dynamical singlets and correlation-assisted peierls transition in VO_2. *Phys. Rev. Lett.* **94**, 026404 (2005).
22. Lechermann, F., Han, Q. & Millis, A. J. Spatial inhomogeneity and the metal-insulator transition in $Ca_3(Ru_{1-x}Ti_x)_2O_7$. *Phys. Rev. Res.* **2**, 033490 (2020).
23. Georges, A., de' Medici, L. & Mravlje, J. Strong correlations from Hund's coupling. *Ann. Rev. Condens. Matter Phys.* **4**, 137 (2013).
24. Georges, A. *Strongly Correlated Electron Materials: Dynamical Mean-Field Theory and Electronic Structure*, (AIP Conference Proceedings 715, 2004) Chap. 3.
25. Lechermann, F. *Charge Self-Consistency in Correlated Electronic Structure Calculations*, (DMFT: From Infinite Dimensions to Real Materials, Forschungszentrum Jülich GmbH, 2018) Chap. 6.
26. Metzner, W. & Vollhardt, D. Correlated Lattice Fermions in $d = \infty$ Dimensions. *Phys. Rev. Lett.* **62**, 324 (1989).
27. Georges, A. & Kotliar, G. Hubbard model in infinite dimensions. *Phys. Rev. B* **45**, 6479 (1992).
28. Georges, A., Kotliar, G., Krauth, W. & Rozenberg, M. J. Dynamical mean-field theory of strongly correlated fermion systems and the limit of infinite dimensions. *Rev. Mod. Phys.* **68**, 13 (1996).
29. Jarrell, M. & Gubernatis, J. E. Bayesian inference and the analytic continuation of imaginary-time quantum Monte Carlo data. *Physics Reports* **269**, 133 (1996).
30. Zgid, D. & Chan, G. K.-L. Dynamical mean-field theory from a quantum chemical perspective. *J. Chem. Phys.* **134**, 094115 (2011).
31. Lin, N., Marianetti, C. A., Millis, A. J. & Reichman, D. R. Dynamical mean-field theory for quantum chemistry. *Phys. Rev. Lett.* **106**, 096402 (2011).
32. Aryasetiawan, F. et al. Frequency-dependent local interactions and low-energy effective models from electronic structure calculations. *Phys. Rev. B* **70**, 195104 (2004).
33. Savrasov, S. Y., Kotliar, G. & Abrahams, E. Correlated electrons in δ-plutonium within a dynamical mean-field picture. *Nature* **410**, 793 (2001).
34. Minár, J. et al. Multiple-scattering formalism for correlated systems: A KKR-DMFT approach. *Phys. Rev. B* **72**, 045125 (2005).
35. Pourovskii, L. V., Amadon, B., Biermann, S. & Georges, A. Self-consistency over the charge density in dynamical mean-field theory: a linear muffin-tin implementation and some physical implications. *Phys. Rev. B* **76**, 235101 (2007).
36. Grieger, D., Piefke, C., Peil, O. E. & Lechermann, F. Approaching finite-temperature phase diagrams of strongly correlated materials: a case study for V_2O_3. *Phys. Rev. B* **86**, 155121 (2012).
37. Amadon, B. et al. Plane-wave based electronic structure calculations for correlated materials using dynamical mean-field theory and projected local orbitals. *Phys. Rev. B* **77**, 205112 (2008).
38. Lechermann, F. Dynamical mean-field theory using Wannier functions: A flexible route to electronic structure calculations of strongly correlated materials. *Phys. Rev. B* **74**, 125120 (2006).
39. Potthoff, M. & Nolting, W. Surface metal-insulator transition in the Hubbard model. *Phys. Rev. B* **59**, 2549 (1999).
40. Elsässer, C. et al. Relativistic effects on ground state properties of 4d and 5d transition metals. *J. Phys.: Condens. Matter* **2**, 4371 (1990).
41. Lechermann, F. Density-functional study of Fe_3Al: LSDA versus GGA. *Phys. Rev. B* **65**, 132104 (2002).
42. Meyer, B., Elsässer, C., Lechermann, F. and Fähnle, M. *FORTRAN 90 Program for Mixed-Basis-Pseudopotential Calculations for Crystals*, Max-Planck-Institut für Metallforschung, Stuttgart (1998).
43. Perdew, J. P., Burke, K. & Ernzerhof, M. Generalized gradient approximation made simple. *Phys. Rev. Lett.* **77**, 3865 (1996).
44. Anisimov, V. I. Full orbital calculation scheme for materials with strongly correlated electrons. *Phys. Rev. B* **71**, 125119 (2005).
45. Korotin, M. A., Anisimov, V. I., Khomskii, D. I. & Sawatzky, G. A. CrO_2: a self-doped double exchange ferromagnet. *Phys. Rev. Lett.* **80**, 4305 (1998).
46. Lechermann, F. Correlation effects on the doped triangular lattice in view of the physics of sodium-Rich Na_xCoO_2. *Phys. Rev. Lett.* **102**, 046403 (2009).
47. Rubtsov, A. N., Savkin, V. V. & Lichtenstein, A. I. Continuous-time quantum Monte Carlo method for fermions. *Phys. Rev. B* **72**, 035122 (2005).
48. Werner, P., Comanac, A., de' Medici, L., Troyer, M. & Millis, A. J. Continuous-time solver for quantum impurity models. *Phys. Rev. Lett.* **97**, 076405 (2006).
49. Parcollet, O. TRIQS: A toolbox for research on interacting quantum systems. *Comput. Phys. Commun.* **196**, 398 (2015).
50. Seth, P., Krivenko, I., Ferrero, M. & Parcollet, O. TRIQS/CTHYB: A continuous-time quantum Monte Carlo hybridisation expansion solver for quantum impurity problems. *Comput. Phys. Commun.* **200**, 274 (2016).

51. Anisimov, V. I., Solovyev, I. V., Korotin, M. A., Czyżyk, M. T. & Sawatzky, G. A. Density-functional theory and NiO photoemission spectra. *Phys. Rev. B* **48**, 16929 (1993).
52. Vidberg, H. J. & Serene, J. W. Solving the Eliashberg equations by means of N-point Padé approximants. *J Low Temp Phys* **29**, 179 (1977).
53. Hicks, C. W. et al. Quantum oscillations and high carrier mobility in the delafossite $PdCoO_2$. *Phys. Rev. Lett.* **109**, 116401 (2012).
54. Moll, P. J. W., Kushwaha, P., Nandi, N., Schmidt, B. & Mackenzie, A. P. Evidence for hydrodynamic electron flow in $PdCoO_2$. *Science* **351**, 1061 (2016).
55. Andreev, A. V., Kivelson, S. A. & Spivak, B. Hydrodynamic description of transport in strongly correlated electron systems. *Phys. Rev. Lett.* **106**, 256804 (2011).
56. Gurzhi, R. Minimum of resistance in impurity-free conductors. *Sov. Phys. JETP* **44**, 771 (1963).
57. Scaffidi, T., Nandi, N., Schmidt, B., Mackenzie, A. P. & Moore, J. E. Hydrodynamic electron flow and hall viscosity. *Phys. Rev. Lett.* **118**, 226601 (2017).
58. Varnavides, G., Jermyn, A. S., Anikeeva, P., Felser, C. & Narang, P. Electron hydrodynamics in anisotropic materials. *Nat. Commun.* **11**, 4710 (2020).
59. Ouyang, S. et al. Correlation of crystal structures, electronic structures, and photocatalytic properties in a series of Ag-based oxides: $AgAlO_2$, $AgCrO_2$, and Ag_2CrO_4. *J. Phys. Chem. C* **112**, 3134 (2008).
60. Mekata, M., Sugino, T., Oohara, A., Oohara, Y. & Yoshizawa, H. Magnetic structure of antiferromagnetic $PdCrO_2$ possible degenerate helices on a rhombohedral lattice. *Physica B* **213**, 221 (1995).
61. Oohara, Y. Magnetic phase transition in $AgCrO_2$. *J. Phys. Soc. Jpn.* **63**, 847 (1994).
62. Seki, S., Onose, Y. & Tokura, Y. Spin-driven ferroelectricity in triangular lattice antiferromagnets $ACrO_2$ (A=Cu, Ag, Li, or Na). *Phys. Rev. Lett.* **101**, 067204 (2008).
63. Eyert, V., Frésard, R. & Maignan, A. On the metallic conductivity of the delafossites $PdCoO_2$ and $PtCoO_2$. *Chem. Mater.* **20**, 2370 (2008).
64. Ong, K. P., Zhang, J., Tse, J. S. & Wu, P. Origin of anisotropy and metallic behavior in delafossite $PdCoO_2$. *Phys. Rev. B* **81**, 115120 (2010).
65. Ong, K. P. & Singh, D. J. Three-dimensional magnetism and coupling to the conduction electrons in $PdCrO_2$. *Phys. Rev. B* **85**, 134403 (2012).
66. Sobota, J. A. Electronic structure of the metallic antiferromagnet $PdCrO_2$ measured by angle-resolved photoemission spectroscopy. *Phys. Rev. B* **88**, 125109 (2013).
67. Gruner, M. E., Eckern, U. & Pentcheva, R. Impact of strain-induced electronic topological transition on the thermoelectric properties of $PtCoO_2$ and $PdCoO_2$. *Phys. Rev. B* **92**, 235140 (2015).
68. Billington, D. Magnetic frustration, short-range correlations and the role of the paramagnetic Fermi surface of $PdCrO_2$. *Sci. Rep.* **5**, 12428 (2015).
69. Noh, H.-J. Anisotropic Electric Conductivity of Delafossite $PdCoO_2$ Studied by Angle-Resolved Photoemission Spectroscopy. *Phys. Rev. Lett.* **102**, 256404 (2009).
70. Ok, J. M. Quantum Oscillations of the Metallic Triangular-Lattice Antiferromagnet $PdCrO_2$. *Phys. Rev. Lett.* **111**, 176405 (2013).
71. Hicks, C. W. Quantum oscillations and magnetic reconstruction in the delafossite $PdCrO_2$. *Phys. Rev. B* **92**, 014425 (2015).
72. Lechermann, F. & Richter, R. Theoretical design of highly correlated electron states in delafossite heterostructures. *Phys. Rev. Research* **2**, 013352 (2020).
73. Takatsu, H., Yoshizawa, H., Yonezawa, S. & Maeno, Y. Critical behavior of the metallic triangular-lattice Heisenberg antiferromagnet $PdCrO_2$. *Phys. Rev. B* **79**, 104424 (2009).
74. Lechermann, F., Körner, W., Urban, D. F. & Elsässer, C. Interplay of charge-transfer and Mott-Hubbard physics approached by an efficient combination of self-interaction correction and dynamical mean-field theory. *Phys. Rev. B* **100**, 115125 (2019).
75. Mott, N. Rare-earth compounds with mixed valencies. *Philosophical Magazine* **30**, 403 (1974).
76. Doniach, S. The Kondo lattice and weak antiferromagnetism. *Physica B* **91**, 231 (1977).
77. Komleva, E. V., Irkhin, V. Y., Solovyev, I. V., Katsnelson, M. I. & Streltsov, S. V. Unconventional magnetism and electronic state in the frustrated layered system $PdCrO_2$. *Phys. Rev. B* **102**, 174438 (2020).
78. Bednorz, J. G. & Müller, K. A. Possible highTc superconductivity in the Ba-La-Cu-O system. *Z. Physik B - Condensed Matter* **64**, 189 (1986).
79. Zubko, P., Gariglio, S., Gabay, M., Ghosez, P. & Triscone, J.-M. Interface physics in complex oxide heterostructures. *Annu. Rev. Condens. Matter Phys.* **2**, 141 (2011).
80. Hwang, H. Y. et al. Emergent phenomena at oxide interfaces. *Nature Materials* **11**, 103 (2012).
81. Mazin, I. I. Theoretical prediction of a strongly correlated Dirac metal. *Nat. Commun.* **5**, 4261 (2014).
82. Ye, L. Massive Dirac fermions in a ferromagnetic kagome metal. *Nature* **555**, 638 (2018).
83. Ghimire, N. J. & Mazin, I. I. Topology and correlations on the kagome lattice. *Nat. Mater.* **19**, 137 (2020).
84. Piefke, C., Boehnke, L., Georges, A. & Lechermann, F. Considerable nonlocal electronic correlations in strongly doped Na_xCoO_2. *Phys. Rev. B* **82**, 165118 (2010).
85. Peil, O. E., Georges, A. & Lechermann, F. Strong correlations enhanced by charge ordering in highly doped cobaltates. *Phys. Rev. Lett.* **107**, 236404 (2011).
86. Wallace, P. R. The band theory of graphite. *Phys. Rev.* **71**, 622 (1947).
87. Li, G. In situ modification of a delafossite-type $PdCoO_2$ bulk single crystal for reversible hydrogen sorption and fast hydrogen evolution. *ACS Energy Lett.* **4**, 2185 (2019).
88. Harada, T., Fujiwara, K. & Tsukazaki, A. Highly conductive $PdCoO_2$ ultrathin films for transparent electrodes. *APL Mater.* **6**, 046107 (2018).
89. Brahlek, M. Growth of metallic delafossite $PdCoO_2$ by molecular beam epitaxy. *Phys. Rev. Materials* **3**, 093401 (2019).
90. Yordanov, P. Large thermopower anisotropy in $PdCoO_2$ thin films. *Phys. Rev. Materials* **3**, 085403 (2019).
91. Sun, J. Growth of $PdCoO_2$ by ozone-assisted molecular-beam epitaxy. *APL Mater.* **7**, 121112 (2019a).
92. Ok, J. M. Pulsed-laser epitaxy of metallic delafossite $PdCrO_2$ films. *APL Mater.* **8**, 051104 (2020).
93. Wei, R. Solution-processable epitaxial metallic delafossite oxide films. *Adv. Funct. Mater.* **30**, 2002375 (2020).
94. Harada, T. et al. Determination of the phase coherence length of $PdCoO_2$ nanostructures by conductance fluctuation analysis. *Phys. Rev. B* **103**, 045123 (2021).
95. Sunko, V. Maximal Rashba-like spin splitting via kinetic-energy-coupled inversion-symmetry breaking. *Nature* **549**, 492 (2017).
96. Mazzola, F. Itinerant ferromagnetism of the Pd-terminated polar surface of $PdCoO_2$. *PNAS* **115**, 12956 (2018).
97. Harada, T. Anomalous Hall effect at the spontaneously electron-doped polar surface of $PdCoO_2$ ultrathin films. *Phys. Rev. Research* **2**, 013282 (2020).
98. Sunko, V. Controlled introduction of defects to delafossite metals by electron irradiation. *Phys. Rev. X* **10**, 021018 (2020b).
99. Tanaka, M., Hasegawa, M. & Takei, H. Growth and characterization of delafossite-type $Pd(Co_{1-x}Mn_x)O_2$ (x=0.04, 0.11) single crystals. *Journal of Crystal Growth* **203**, 400 (1999).
100. Wawrzyńska, E. Orbital degeneracy removed by charge order in triangular antiferromagnet $AgNiO_2$. *Phys. Rev. Lett.* **99**, 157204 (2007).
101. Ralko, A., Merino, J. & Fratini, S. Pinball liquid phase from Hund's coupling in frustrated transition-metal oxides. *Phys. Rev. B* **91**, 165139 (2015).
102. Kan, E. J., Xiang, H. J., Zhang, Y., Lee, C. & Whangbo, M.-H. Density-functional analysis of spin exchange and ferroelectric polarization in $AgCrO_2$. *Phys. Rev. B* **80**, 104417 (2009).
103. Arsenijević, S. Anomalous magnetothermopower in a metallic frustrated antiferromagnet. *Phys. Rev. Lett.* **116**, 087202 (2016).
104. Ghannadzadeh, S. Simultaneous loss of interlayer coherence and long-range magnetism in quasi-two-dimensional $PdCrO_2$. *Nat. Commun.* **8**, 15001 (2017).
105. Le, M. D. Magnetic interactions in $PdCrO_2$ and their effects on its magnetic structure. *Phys. Rev. B* **98**, 024429 (2018).
106. Sun, D. Magnetic frustration and spontaneous rotational symmetry breaking in $PdCrO_2$. *Phys. Rev. B* **100**, 094414 (2019b).
107. Park, C. & Yu, J. *Twisted double-layer chiral spin structures in anti-ferromagnetic delafossite $PdCrO_2$*, Preprint at https://arxiv.org/abs/2001.06834 (2020).
108. Kudasov, Y. B. Skew band structure and anomalous conductivity of $PdCrO_2$, Preprint at https://arxiv.org/abs/2006.05453 (2020).
109. Boehnke, L. & Lechermann, F. Competing orders in Na_xCoO_2 from strong correlations on a two-particle level. *Phys. Rev. B* **85**, 115128 (2012).

ACKNOWLEDGEMENTS

We are indebted to H. O. Jeschke, P. D. C. King, I. Krivenko, A. P. Mackenzie, L. Pourovskii, R. Richter, A. W. Rost, V. Sunko, and P. Wahl for helpful discussions on various facets of delafossites as well as on computational aspects. Financial support from the DFG LE-2446/4-1 project "Design of strongly correlated materials" and the Psi-k network is acknowledged. Computations were performed at the JUWELS Cluster of the Jülich Supercomputing Centre (JSC) under project number hhh08.

AUTHOR CONTRIBUTIONS

F.L. set up the problem, conducted the calculations, collected the data, analyzed the results and wrote the manuscript.

COMPETING INTERESTS

The author declares no competing interests.

ADDITIONAL INFORMATION

Correspondence and requests for materials should be addressed to F.L.

Reprints and permission information is available at http://www.nature.com/reprints

Publisher's note Springer Nature remains neutral with regard to jurisdictional claims in published maps and institutional affiliations.